Efficient SARS-CoV-2 detection utilizing chitin-immobilized nanobodies synthesized in *Ustilago maydis*

Magnus Philipp[1], Lisa Müller[2], Marcel Andrée[2], Kai P. Hussnaetter[1], Heiner Schaal[2], Michael Feldbrügge[1] and Kerstin Schipper[1*]

[1] Institute for Microbiology, Heinrich Heine University Düsseldorf, Universitätsstraße 1, 40225 Düsseldorf, Germany

[2] Institute of Virology, Medical Faculty, Heinrich Heine University Düsseldorf, Universitätsstraße 1, 40225 Düsseldorf, Germany

[*] Corresponding author:

Kerstin Schipper

E-mail: kerstin.schipper@uni-duesseldorf.de

Abstract

The COVID-19 pandemic has greatly impacted the global economy and health care systems, illustrating the urgent need for timely and inexpensive responses to a pandemic threat in the form of vaccines and antigen tests. The causative agent of COVID-19 is SARS-CoV-2. The spike protein on the virus surface interacts with the human angiotensin-converting enzyme (ACE2) via the so-called receptor binding domain (RBD), facilitating virus entry. The RBD thus represents a prime target for vaccines, therapeutic antibodies, and antigen test systems. Currently, antigen testing is mostly conducted by qualitative flow chromatography or via quantitative ELISA-type assays. The latter mostly utilize materials like protein-adhesive polymers and gold or latex particles. Here we present an alternative ELISA approach using inexpensive materials and permitting quick detection based on components produced in the microbial model *Ustilago maydis*. In this fungus, heterologous proteins like biopharmaceuticals can be exported by fusion to unconventionally secreted chitinase Cts1. As a unique feature, the carrier chitinase binds to chitin allowing its additional use as a purification or immobilization tag. In this study, we produced different mono- and bivalent SARS-CoV-2 nanobodies

31 directed against the viral RBD as Cts1 fusions and screened their RBD binding affinity *in vitro* and *in*

32 *vivo*. Functional nanobody-Cts1 fusions were immobilized on chitin forming an RBD tethering surface.

33 This provides a solid base for future development of an inexpensive antigen test utilizing

34 unconventionally secreted nanobodies as RBD trap and a matching ubiquitous and biogenic surface

35 for immobilization.

36

1   Introduction

38 The current COVID-19 pandemic challenges not only global healthcare systems and economies but

39 has also underlined the strong demand for novel and versatile strategies to fight viral pandemics. In

40 this regard, major innovations have already been driven by the pandemic, exemplified by the prompt

41 development of mRNA-based vaccines (Kudlay and Svistunov 2022). Furthermore, the adaptation of

42 monoclonal antibody therapeutics formerly mostly used in cancer patients for the treatment of COVID-

43 19 represented an important step (Sun and Ho 2020, Bierle et al. 2021).

44   COVID-19 is caused by SARS-CoV-2. With the onset of the pandemic, the structure of the

45 virus has been elucidated both on RNA (Jain et al. 2020) and protein level (Korber et al. 2020, Ou et

46 al. 2020, Walls et al. 2020, Wrapp et al. 2020b). The spike protein complex was identified as a key

47 player, as it is not only exposed on the surface of the viral particle, but also enables the attachment of

48 the virus to the host cell via the human Angiotensin receptor 2 (ACE2) (Wang et al. 2020a). This

49 mechanism has also been observed for other beta corona viruses like SARS-CoV (Hulswit et al. 2016).

50 Spike proteins of these viral species usually consist of the two main subunits S2 and S1. S2 mainly

51 serves as anchor of the protein in the viral membrane and also mediates fusion of the viral envelope

52 and the host cell membrane (Hulswit et al. 2016). S1 is responsible for ACE2 binding (Wang et al.

53 2020a). Corona virus S1 proteins are generally organized into four domains, of which domains A and

54 B form the receptor binding domain (RBD) which mediates ACE2 binding (Li et al. 2003, Wang et al.

55 2020a). The B subdomain of the RBD carries an extended loop that is highly variable among corona

56 virus species and therefore also referred to as hypervariable region (Kirchdoerfer et al. 2016). All

57 SARS-CoV-2 variants of concern that have been structurally elucidated to date (B.1.1.7 Alpha, B.1.351

58 Beta and B.1617 Delta and B.1.1.529 Omicron) carry mutations within the RBD domain that are

59 assumed to play a role in infectivity and transmissibility of the virus (Baral et al. 2021, Torjesen 2021,

60 VanBlargan et al. 2022). Therefore, the spike protein and especially its RBD domain are key targets

61 for the development of therapeutics and vaccines.

62   The majority of vaccines cleared for use to date use an mRNA template of the spike protein

63   that is translated in the host to evoke an immune response (Callaway 2020, Fernandes et al. 2022).

64   However, since it was realized that vaccinated persons can still be infected with and spread SARS-

65   CoV-2, there is a strong pressure to further develop test systems and therapeutics for a multi-layered

66   strategy for COVID-19 treatment and control of SARS-CoV-2 spreading. Antibodies are key to both

67   test systems and drug development. *Camelidae* and shark derived single heavy chain antibodies and

68   derived nanobodies are emerging as potent alternatives to conventional antibodies (Muyldermans

69   2013, Salvador et al. 2019). *Camelidae* type antibodies only carry a heavy chain on their IgG scaffold

70   as opposed to the light- and heavy chain of regular mammalian antibodies (Muyldermans 2013). This

71   heavy chain alone (the so-called nanobody) can be quickly adapted to novel targets such as SARS-

72   CoV-2 and production in microbial hosts is straightforward (Muyldermans et al. 2009, Wrapp et al.

73   2020a). Nanobodies have been shown to bind ligands in the nanomolar range and are stable under

74   conditions of chemical and heat induced stress (Muyldermans 2013), which makes them promising

75   molecules for widespread antigen testing. To this end several SARS-CoV-2 nanobodies engineered

76   synthetically via phage display or generated directly by immunization of llamas, alpacas, and sharks

77   have been published (Custodio et al. 2020, Gauhar et al. 2021, König et al. 2021).

78   We utilize the yeast form of the microbial model *Ustilago maydis* to produce heterologous

79   proteins including alternative antibody formats like single chain variable fragments (scFvs) and

80   nanobodies (Sarkari et al. 2014, Terfrüchte et al. 2017). Recently, we also established production of

81   functional synthetic anti-SARS-CoV-2 nanobodies as a proof-of-principle for protein

82   biopharmaceuticals (Philipp et al. 2021). For secretion of heterologous target proteins, a recently

83   described unconventional secretion mechanism used by fungus to export chitinase Cts1 during

84   cytokinesis is exploited (Reindl et al. 2019). Therefore, proteins of interest are fused to Cts1 which

85   serves as a carrier for the export into the culture supernatant (Stock et al. 2012, Stock et al. 2016). Cts1

86   exhibits chitin binding activity making it a potential build-in immobilization- and purification tag

87   (Terfrüchte et al. 2017). In addition, Jps1, a potential anchoring factor needed for Cts1 secretion is

88   released into the culture medium and can be employed as alternative carrier (Philipp et al. 2021). Of

89   note, proteins directed to the unconventional secretion pathway are not decorated with potentially

90   harmful post translational protein modifications such as *N*-glycosylation which could lead to strong

91   reactions in patients when proteins are applied as biopharmaceuticals (Stock et al. 2012).

92   Here, we exploited the dual functionality of chitinase Cts1 to produce different published SARS-

93   CoV-2 nanobody versions via unconventional Cts1 secretion in *U. maydis*. Nanobody fusions were

94   screened for their antigen binding activity *in vitro* and *in vivo*. Using the most promising binders, we

95   established a novel strategy of RBD detection using a chitin surface for immobilization. In the future,

96   these components can be combined to design a novel inexpensive and versatile virus detection system

97   based on fungal compounds and a cognate biogenic chitin surface.

98

99   2   Results

100 2.1 Functional comparison of SARS-CoV-2 nanobody variants produced by
101   unconventional secretion

102   Recently, we established Jps1 as an alternative carrier for heterologous proteins using the

103   production of synthetic nanobodies against SARS-CoV-2 as a test case. We were successful in

104   generating a functional bivalent nanobody directed against SARS-CoV-2 spike protein RBD (Sy$^{68/15}$-

105   Jps1) (Philipp et al. 2021). However, nanobody export mediated by Cts1 is also of great interest due to

106   its natural ability in mediating both the export of heterologous proteins and chitin binding. The latter

107   property is of potential high value with respect to protein purification and immobilization. Thus, to test

108   the dual applicability of Cts1, we first screened different nanobody-Cts1 fusions for their expression,

109   unconventional secretion and binding activity against SARS-CoV-2 RBD using Sy$^{68/15}$-Jps1 as a

110   benchmark (Fig. 1A). To this end four different strains were generated that produce anti-RBD

111   nanobody versions fused to Cts1. These nanobody versions included the two synthetic nanobodies

112   generated by Wagner et al. (2020) as single entities (Sy^{15}-Cts1, Sy^{68}-Cts1) and two llama-derived

113   nanobodies VHH E and VHH V (here termed VHH^E and VHH^V) generated by König et al. (2021)

114   (VHH^E-Cts1, VHH^V-Cts1). In addition, a strain expressing a hetero bivalent version, pairing VHH^E

115   with VHH^V, was designed, since these were shown to display synergistic activity (König et al. 2021)

116   (VHH^{VE}-Cts1). Finally, a strain for production of a double mono bivalent VHH^E version was generated

117   to test the binding capability of dimers with identical antigen binding sites (VHH^{EE}-Cts1). The

118   published synthetic nanobody versions Sy$^{68/15}$-Cts1 (no antigen binding activity) and bivalent Sy$^{68/15}$-

119   Jps1 (alternative carrier; shows binding activity), pairing two synthetic nanobodies with different

120   antigen binding sites, served as controls (Philipp et al. 2021). *U. maydis* expression strains for all

121   protein versions were generated in the background of laboratory strain AB33P8Δ lacking eight

122   extracellular proteases to optimize secretory yield (Terfrüchte et al. 2018). Expression and secretion of

123   all versions was investigated via Western blot analyses. In cell extracts fusion proteins of the expected

124   sizes were present for all variants, however, huge differences in expression level were observed. The

125   analysis of culture supernatants confirmed sufficient secretion for the variants Sy^{15}-Cts1, VHH^E-Cts1,

126   VHH^V-Cts1, VHH^{EE}-Cts1 and Sy$^{68/15}$-Jps1, again displaying strong variation in the detected amounts

127   (Fig. 1 B, Suppl. Fig. 1 A, B). To test for RBD binding activity, cell extracts of all strains containing

128   nanobody-Cts1 fusions were subjected to direct ELISA assays, using recombinant RBD as a bait and

129   a commercial antibody sandwich for detection. The strongest binding was achieved for VHH^{EE}-Cts1

130   and Sy$^{68/15}$-Jps1 while VHH^{E}-Cts1 showed about half the signal intensity. All other variants lacked

131   clear volumetric binding activity (Fig. 1 C, Suppl. Fig. 1 C). Overall, significant binding activity could

132   be demonstrated for 3 of the 8 nanobody variants and binding capabilities of nanobodies were improved

133   in the multimerized variant of VHH^{EE}-Cts1.

134   To further substantiate the results, the three most promising nanobody versions VHH^{EE}-Cts1,

135   VHH^{E}-Cts1 and Sy$^{68/15}$-Jps1 were purified and subjected to direct ELISA against the full length S1

136   protein using an Anti-SARS-CoV-2 QuantiVac ELISA-kit including controls (Fig. 1 D). All variants

137   depicted significant binding activity with VHH^{E}-Cts1 binding at concentrations of 5 ng/µl and 10 ng/µl

138   and both VHH^{EE}-Cts1 and Sy$^{68/15}$-Jps1 showing more than two-fold elevated binding compared to

139   VHH^{E}-Cts1. In essence, two functional nanobody-Cts1-fusion proteins were obtained which were

140   comparable to the current benchmark Sy$^{68/15}$-Jps1, recognizing both recombinant RBD and full length

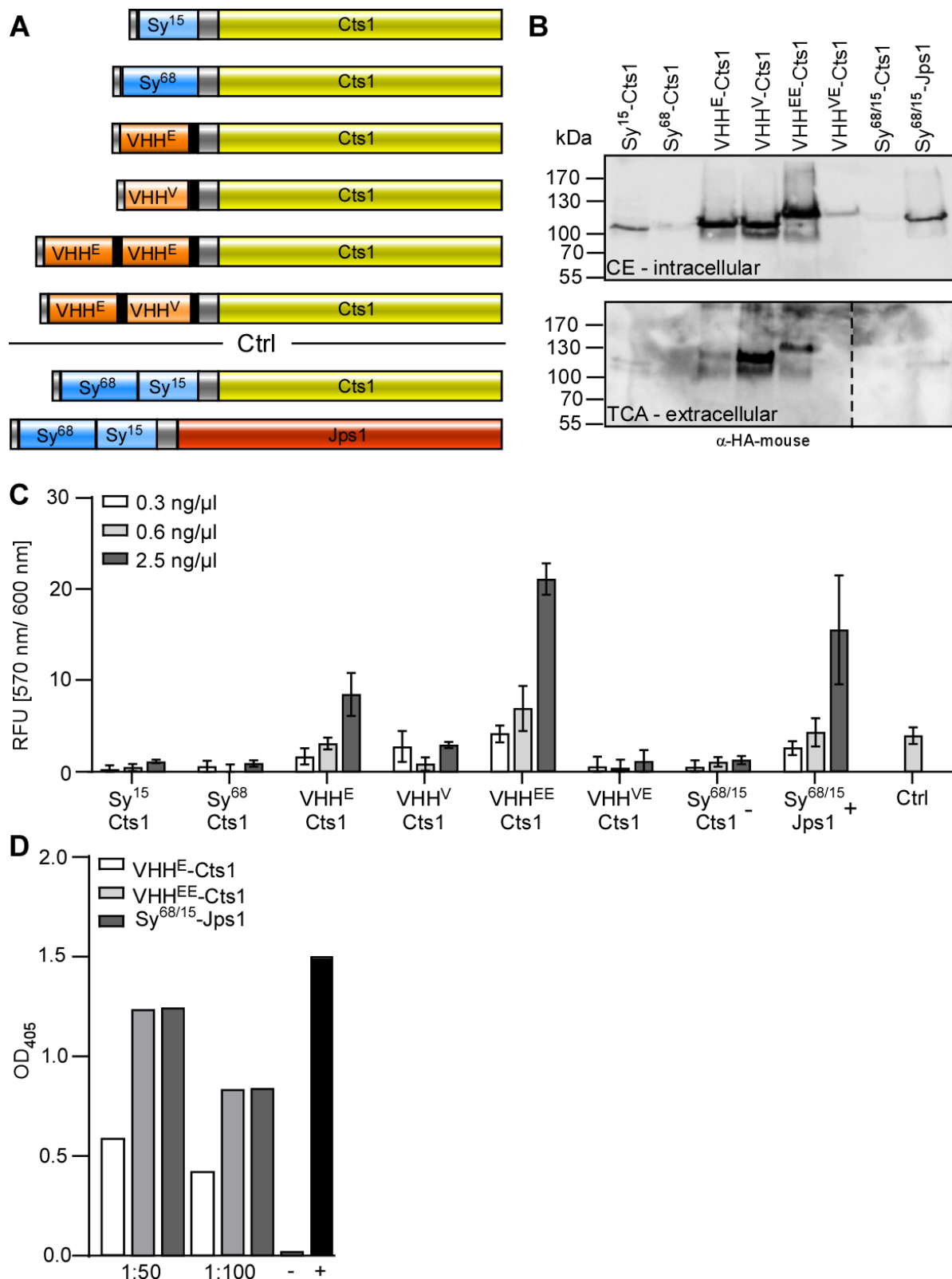141   S1 protein.

142

143

144

145

146

Figure 1: Functional screen of anti-SARS-CoV-2 nanobody-Cts1-fusion variants. (A) Schematic representation of nanobody protein variants fused to chitinase Cts1 as a carrier for unconventional secretion. Synthetic nanobodies Sy^{15} and Sy^{68} as well as llama-derived nanobodies VHH^E, VHH^V and bivalent VHH^{VE} as well as a tandem VHH^E (VHH^{EE}) were fused to Cts1 (yellow) via an HA-tag (grey) for detection. A His-tag (grey) was added at the N-terminus as a purification

152   tag. In the case of the VHH^E and VHH^V nanobodies GS-linkers (black) introduced by (König et al. 2021) were placed

153   between individual nanobodies and between the nanobodies and Cts1. Sy$^{68/15}$-Cts1 and Sy$^{68/15}$-Jps1 (Philipp et al., 2021)

154   dealt as negative and positive control, respectively. Protein schemes drawn to scale. **(B)** Western blot analysis to detect

155   nanobody expression and secretion levels. Top, cell extracts: 10 µg of cell extracts producing the indicated protein variants

156   were subjected to Western blot analysis. Bottom, culture supernatants of strains producing indicated protein variants.

157   Proteins were enriched from the supernatant via TCA precipitation, the HA tag was used for detection. Nanobody-Cts1-

158   fusions were detected using an HA-mouse antibody and migrate slightly above their expected sizes around 100 kDa. **(C)**

159   Direct ELISA of nanobody-Cts1-fusions against 1 µg/well of RBD domain coated to ELISA plate and detected by a

160   sandwich of anti-HA (mouse) and an anti-mouse-HRP conjugate. Cell extracts of indicated expression strains were added

161   to wells in serial dilutions of 0.3 ng/µl, 0.6 ng/µl and 2.5 ng/µl. The experiment was carried out in three biological replicates.

162   Error bars depict standard deviation. **(D)** Direct ELISA of nanobody-Cts1 fusions against full length spike protein directly

163   detected with an anti-HA-HRP conjugate. Purified nanobody-fusions (100 µg/ml) were added to wells in dilutions of 1:50

164   and 1:100 in technical triplicates. One biological replicate is shown. (+) and (-) indicate controls included in QuantiVac

165   ELISA-kit.

166

2.2 *In vivo* activity of nanobody-Cts1 fusions

168   To determine if *in vitro* binding to SARS-CoV-2 RBD translates to binding or even virus neutralization

169   *in vivo,* adjusted neutralization assays were applied. These assays are widely used to test sera of

170   vaccinated or recovered patients for SARS-CoV-2 neutralizing antibodies (Matusali et al. 2021, Müller

171   et al. 2021). In this adjusted neutralization assay, infectious SARS-CoV-2 viral particles were diluted

172   two-fold starting at 100 TCID50 (tissue culture infectious dose 50). Dilutions were then pre-incubated

173   with the purified functional nanobody variants VHH^E-Cts1, VHH^{EE}-Cts1 and Sy$^{68/15}$-Jps1. The

174   mixtures were subsequently used to inoculate Vero cell cultures displaying the ACE2 receptor on their

175   surface to analyze viral replication. To quantify infection and neutralization, qPCR analysis was carried

176   out for each replicate at the onset of infection and at three days' post infection. VHH^E-Cts1 showed no

177   virus neutralization with strongly declining Ct values between t0 and t3, indicating a replicative

178   infection. VHH^{EE}-Cts1 on the other hand showed neutralization up to 25 TCID50 and Sy$^{68/15}$-Jps1 up

179   to 50 TCID50 as indicated by stable Ct values (Fig. 2 A). These results confirm the functionality of the

180   nanobody fusions VHH^{EE}-Cts1 and Sy$^{68/15}$-Jps1 even towards infectious virus. Given that binding does

181   not necessarily reflect neutralization, but neutralization definitely includes binding, this also confirms

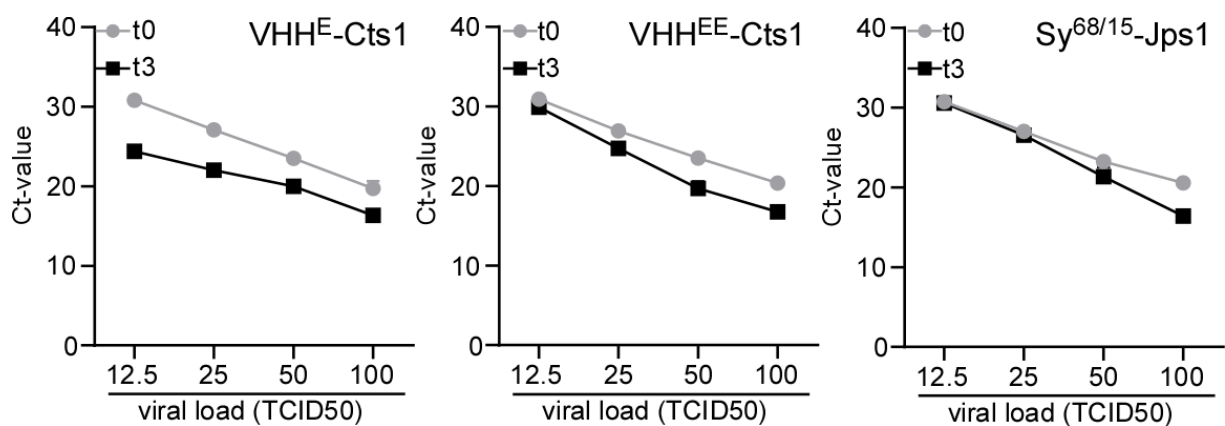182   that these two versions are capable of binding SARS-CoV-2 *in vivo*.

183

Figure 2: Neutralization assays conducted with anti-SARS-CoV-2 nanobody fusions produced in *U. maydis*. (B) qPCR analysis of infected mammalian cells to detect viral RNA in cell cultures treated with purified nanobody fusions/SARS-CoV-2 mixtures. Ct-values of samples at the onset of infection (t0) and three days' post infection (t3) are depicted for each viral load and the respective applied nanobody fusion. Strong differences between Ct values of t0 and t3 indicate infection. Mean values of three biological replicates are depicted.

2.3   Characterization of Cts1 chitin binding and immobilization

Cts1 is capable of binding to chitin-coated surfaces like chitin magnetic beads without obvious degradation of the polymer (Terfrüchte et al. 2017). This observation could be developed into a strategy for a novel antigen test using an inexpensive surface based on bulk chitin obtained from crab shell or insects for immobilization of Cts1-nanobody fusions. To test chitin immobilization, we first recapitulated chitin binding on chitin beads using purified recombinant Cts1 (Fig. 3 A). Therefore, beads were mixed with recombinant Cts1 produced in *Escherichia coli*. After thorough washing, Cts1 was eluted from the beads, indicating stable binding and confirming previous results (Terfrüchte et al. 2017). Analysis of the fractions indicated that a significant amount of the protein was lost in the flow-through, suggesting that binding efficiency could be further improved in the future (Fig. 3 B). Next, β-glucuronidase (Gus)-Cts1 (Stock et al. 2012) obtained from *U. maydis* was used to quantify previous results (Terfrüchte et al. 2017) in the native system and to further characterize the chitin binding capacity of fusion proteins. Gus-Jps1 (Reindl et al. 2020), which is not predicted to bind to chitin, was used as a negative control (Fig. 3 C). Chitin beads were coated with the respective Gus-fusion proteins purified from *U. maydis* while washing and elution procedures were kept consistent to experiments carried out with recombinant Cts1. Indeed, Gus-Cts1 bound to chitin beads while no binding was observed for Gus-Jps1, confirming the binding capability of N-terminal Cts1-fusion proteins (Fig. 3 D). Quantification of signal intensities of the different fractions obtained in both experiments indicated that about 44% of the recombinant Cts1 and 68% of the native Gus-Cts1-fusion protein was captured

210   by the beads (Fig. 3 E). To finally assay if the fusion protein is functional after immobilization, Gus

211   activity was determined on chitin beads previously incubated with raw cell extracts of the Gus-Cts1

212   expression strain. Activity could specifically be detected on beads incubated with Gus-Cts1 containing

213   cell extracts while the controls showed only background activity (Fig. 3 F). In essence, functional Cts1-

214   fusion proteins can be immobilized on chitin beads and immobilization can even be achieved directly

215   from raw cell extracts.

216

218   **Figure 3: Chitin binding capabilities of Cts1 and Cts1-fusion proteins. (A)** Experimental setup for initial Cts1 chitin

219   binding experiments. *E. coli* derived, purified Cts1 (yellow) was coated to magnetic chitin beads, washed and subsequently

220   eluted by boiling. **(B)** Coomassie-stained SDS-PAGE of different fractions obtained in the binding studies with recombinant

221   Cts1 from *E. coli*: input (In), flow-through (FT), wash (W1 and W2) and elution (Elu) fractions of the experiment. **(C)**

222   Experimental setup for Cts1 chitin binding experiments using *U. maydis* derived Gus-fusion proteins. Gus-Cts1 (purple-

223 yellow) was coated to chitin beads, while a second set of beads treated with Gus-Jps1 (purple-red) dealt as a negative

224 control. **(D)** Western blot analysis of input (In), flow-through (FT), wash (W1 and W2) and elution (Elu) fractions of

225 purified Gus-Cts1 and Gus-Jps1-fusion protein incubated with chitin beads. **(E)** Relative quantification of SDS-PAGE and

226 Western blot depicted in panels B and D. **(F)** On-bead Gus assays conducted with cell extracts of Gus-Cts1 and Gus-Jps1

227 incubated with chitin beads. After washing a Gus activity assay was conducted. Conversion from 4-MUG to 4-MU was

228 monitored for 1 h. Cell extracts with Gus-Jps1 and of the progenitor strain (Ctrl) dealt as a negative control. Mean values

229 of three biological replicates are shown. Error bars depict standard deviation.

2.4 Assessing the potential of anti-SARS-CoV-2 nanobody-Cts1 fusions for RBD capturing and chitin binding

232 To determine the capturing capabilities of the most promising nanobody variants VHH^E-Cts1

233 and VHH^E-Cts1, sandwich immunosorbent assays were conducted both on ELISA plates and non-

234 classically on chitin beads. Sy$^{68/15}$-Jps1 dealt as a control for both assays as it should show activity in

235 plate-based ELISA but not on a chitin surface. In the first experiment, purified VHH^E-Cts1, VHH^{EE}-

236 Cts1 and Sy$^{68/15}$-Jps1 were coated to ELISA plates, incubated with serial dilutions of recombinant RBD

237 and subsequently detected by a commercial RBD antibody and a cognate HRP conjugate (Fig. 4 A). In

238 this plate-based ELISA all three nanobody variants were capable of capturing the RBD, however, only

239 the most potent versions VHH^{EE}-Cts1 and Sy$^{68/15}$-Jps1 showed volumetric activity for serial RBD

240 dilutions. As observed in the direct ELISA, VHH^{EE}-Cts1 showed the strongest binding capability even

241 at the lowest RBD concentration of 0.1 ng/µl after a detection time of 10 min, showing significantly

242 stronger binding than VHH^E-Cts1 which did neither reveal significant binding at 0.1 ng/µl nor

243 volumetric activity with rising concentrations (Fig. 4 B). To determine if detection of RBD domain at

244 similar concentrations can also be achieved using a chitin surface, chitin beads were incubated with

245 purified VHH^E-Cts1, VHH^{EE}-Cts1 and Sy$^{68/15}$-Jps1, mixed with RBD and again binding was detected

246 using commercial antibodies (Fig. 4 C). Activity was obtained for both VHH^E-Cts1 and VHH^{EE}-Cts1,

247 while no significant signal could be detected for Sy$^{68/15}$-Jps1. As observed before, values for VHH^{EE}-

248 Cts1 were about doubled compared to those for VHH^E-Cts1 (Fig. 4 D). In summary, these results

249 demonstrate the potential of chitin-based ELISA using SARS-CoV-2 nanobody-Cts1-fusions and its

250 specificity for the bifunctional Cts1 dealing as carrier and anchor for immobilization.
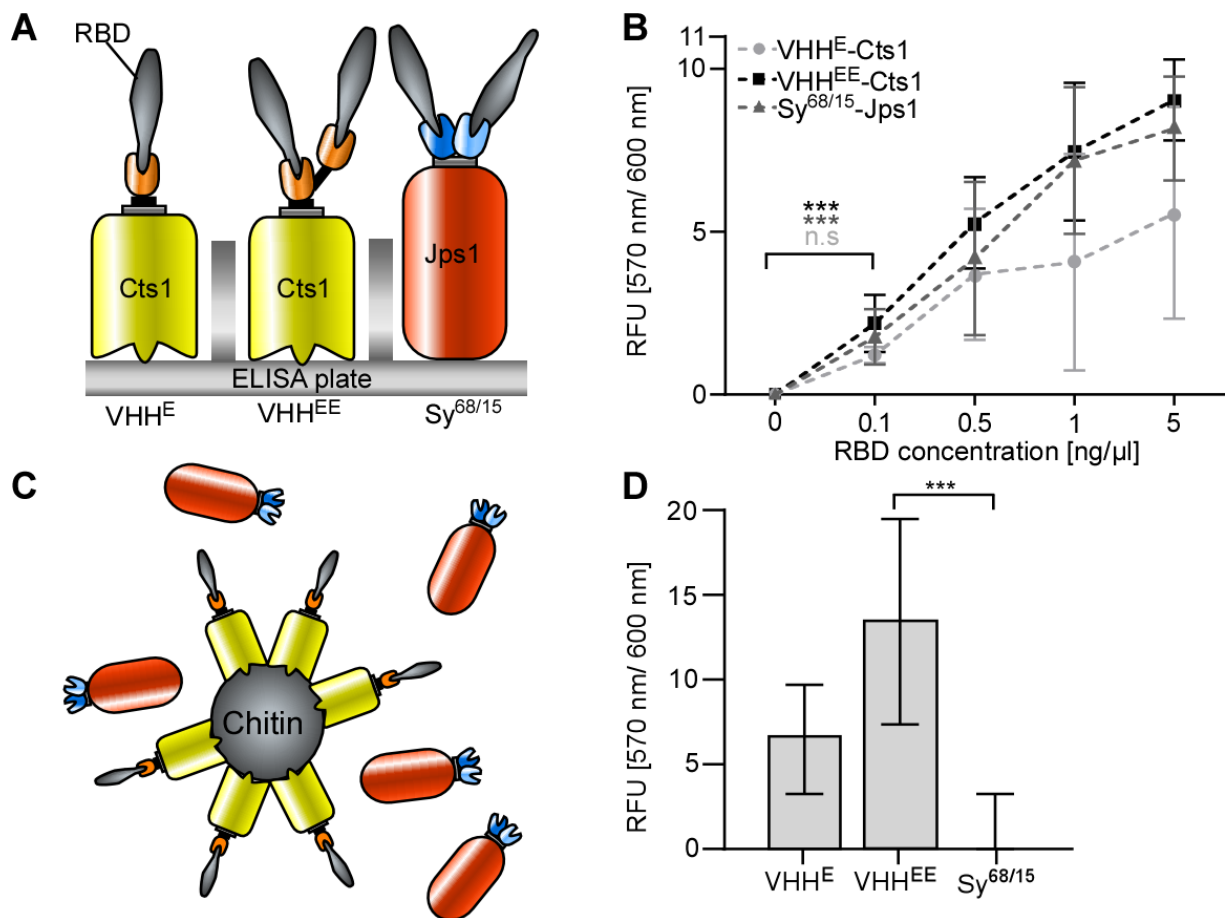
251

Figure 4: Plate-and chitin-based sandwich ELISA using Cts1-nanobody fusions for detection of SARS-CoV-2 RBD. (A) Experimental setup of plate-based sandwich ELISA. The indicated nanobody-Cts1 fusions were used as capture antibodies for serial dilutions of recombinant SARS-CoV-2 RBD (grey). (B) Quantitative results of plate-based sandwich ELISA. RBD (grey) was detected using an anti-RBD-(mouse) antibody and an anti-mouse-HRP conjugate. Mean values of three biological replicates are shown. Error bars depict standard deviation. Definition of statistical significance (***), p-value < 0.05. (C) Experimental setup of chitin-based sandwich ELISA test. The indicated nanobody-Cts1 fusions were coated to chitin beads to serve as capturing nanobodies, while $Sy^{68/15}$-Jps1 dealt as negative control that is unable to bind to chitin. (D) Quantitative results of chitin-based sandwich ELISA. RBD was detected using an anti-RBD (mouse) antibody and anti-mouse-HRP conjugate. $Sy^{68/15}$-Jps1 dealt as a negative control. Mean values of three biological replicates are shown. Error bars depict standard deviation. Definition of statistical significance (***), p-value < 0.05.

To further characterize the RBD capturing capabilities of the chitin-based detection system, the volumetric binding activity of the system was determined. Based on previous results, VHH^{EE}-Cts1 was chosen as the most potent capturing nanobody. To this end, chitin beads were loaded with purified VHH^{EE}-Cts1, subsequently incubated with recombinant RBD in serial dilutions and detected with a commercial antibody sandwich as described above (Fig. 5 A). A colorimetric reaction was obtained within a timeframe of two minutes, reflecting the rising input of the commercial RBD (Fig. 5 B).

270   Quantitative fluorescence measurements of the samples confirmed these visual results (Fig. 5 C).

271   Hence, overall, volumetric detection of SARS-CoV-2 RBD on a chitin surface is feasible, sensitive in

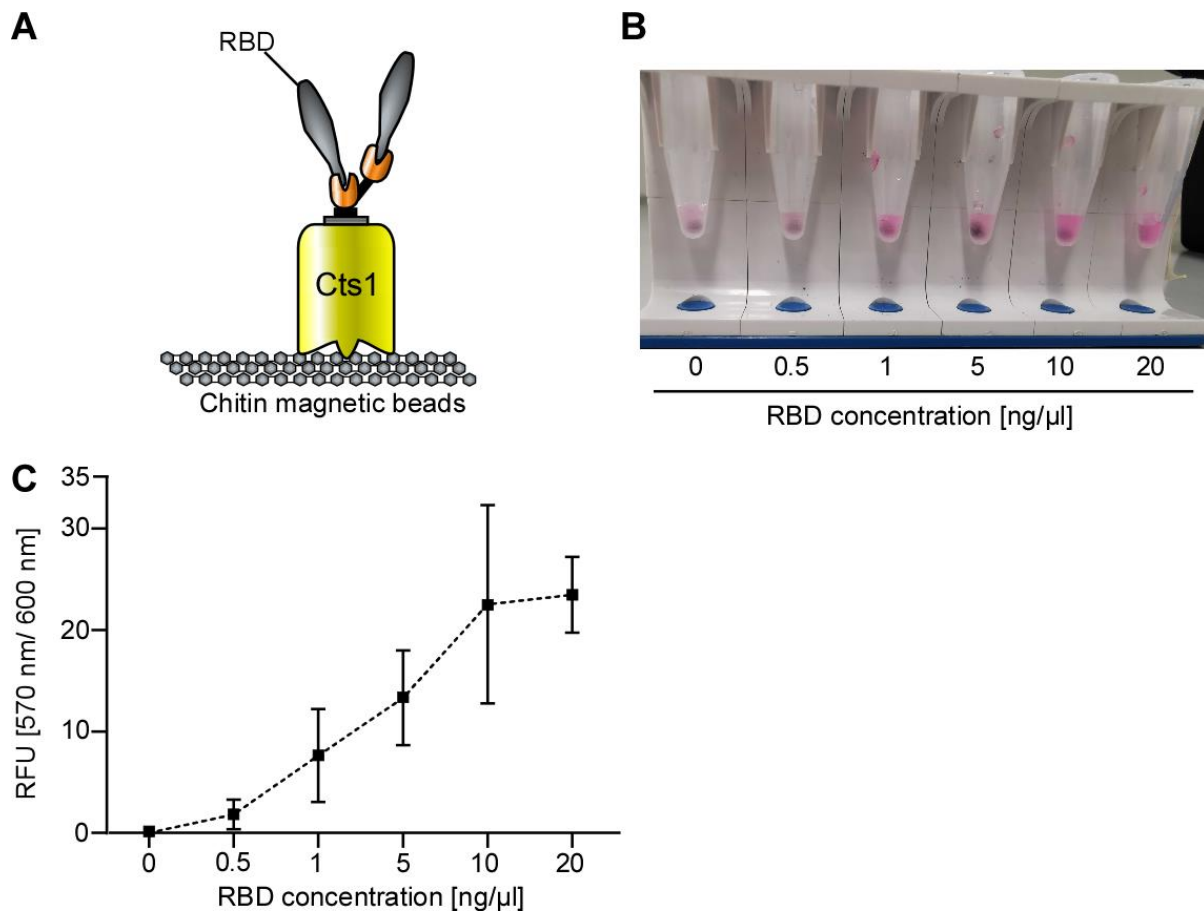272   the nanomolar range and in the given setup even faster than on a conventional ELISA plate.

274   **Figure 5: Chitin-based antigen test. (A)** Setup of chitin-based ELISA. VHH[EE]-Cts1 binds to the chitin magnetic beads

275   and is used as capture antibody for SARS-CoV-2 RBD. **(B)** RBD was added to VHH[EE]-Cts1 coated magnetic chitin beads

276   in serial dilutions and subsequently detected using anti RBD (mouse) and anti-mouse-HRP antibodies. Picture depicts one

277   representative replicate of the observed colorimetric reaction in reaction tubes. **(C)** Quantitative read-out of fluorescence

278   measurements from chitin beads coated with VHH[EE]-Cts1, treated with serial dilutions of SARS-CoV-2 RBD. Mean values

279   of three biological replicates are shown. Error bars depict standard deviation.

3   Discussion

283   The aim of this study was to expand the repertoire of pharmaceutically relevant proteins produced

284   in *U. maydis* towards versatile nanobodies for virus detection. To this end, Cts1-mediated secretion of

285   active camelid-derived single- and bivalent nanobodies directed against the SARS-CoV-2 RBD was

286   achieved. As an important strategical step towards industrial application, the produced nanobody

fusions were immobilized on chitin, exploiting the natural capabilities of Cts1 and thus enabling detection of the cognate antigen via chitin-based ELISA.

The utilization of protein tags like Cts1 to export "passenger" proteins or peptides is a routine strategy in both bacterial and fungal hosts (Fleissner and Dersch 2010). Classical carriers are extracellular proteins that are naturally secreted in very high amounts and can be used as export proteins to guarantee high yields of secreted fusion protein. One such example are carbohydrate-active proteins like CBH1 from *Trichoderma reesei* (Zhong et al. 2011). As a positive side-effect, these protein tags can even enhance the solubility like shown for carbohydrate-binding module 66 (CBM66) in *E. coli* (Ko et al. 2021). In our study, different combinations of nanobody and Cts1 carrier resulted in varying levels of expression, secretion and activity. In addition, we observed a strong impact of the carrier choice on activity of the fused nanobody, confirming our earlier study (Philipp et al. 2021). While this underlines the necessity of a screening step of several constructs for each nanobody, it is in line with results obtained in other carrier based secretion systems (Wang et al. 2020b).

Similarly, also multiple powerful tags for protein purification and immobilization exist with the polyhistidin, the haemagglutinin or the SUMO tag as a few important examples (Porath et al. 1975, Field et al. 1988, Guerrero et al. 2015). The IMPACT system (New England Biolabs) even exploits a chitin-binding protein tag derived from *Mycobacterium xenopi* GyrA for protein purification with the intein tag (Chong et al. 1997, Chong et al. 1998). Importantly, in our system, chitinase Cts1 mediates both export and immobilization of the heterologous proteins. Thus, while normally carriers and tags for purification or immobilization are separated, Cts1 intrinsically combines both properties. This unique strategy will enable a very streamlined process design in the future.

Currently, we are using affinity chromatography to purify the Cts1-fusion proteins. In the future, the development of *in-situ* purification strategies for Cts1-fusion proteins from culture supernatant could greatly ease the purification process and thereby lower production costs of biopharmaceuticals. Similar non chromatographic purification processes have already proven successful using GST, biotin and streptavidin coated magnetic particles to purify protein from *E. coli cell* lysates (Franzreb et al. 2006) and supernatants (Fernandes et al. 2016) but also from human serum plasma (Santos et al. 2020).

In previous studies we had shown that chitin-coated beads are applicable for the purification of Cts1-fusion proteins (Terfrüchte et al. 2017). Now we expand on that and developed this interaction for nanobody immobilization in immunoassays. Since protein immobilization is generally achieved via protein adhesive polymers and not by specific protein-molecule interaction (Lin 2015, Andryukov 2020) this provides a novel tool towards inexpensive surface coating. The use of bio-based polymers

320   for immobilization is of utmost interest since it allows for reduction of antigen test pricing and use of

321   sustainable and inexpensive resources. To this end a similar study achieved SARS-CoV-2 detection

322   based on nanobody immobilization on cellulose, albeit without using the immobilization tag for export

323   at the same time (Sun et al. 2022).

324   Importantly, RBD capture capability of VHH^{EE}-Cts1 in this study could be shown at

325   concentrations in the low nanomolar range of 2.6 nm (0.1 ng/µl) in plate based ELISA, which is in the

326   described range of other anti-RBD nanobodies between 0.9 nm and 30 nM (Weinstein et al. 2022),

327   (Huo et al. 2020), (König et al. 2021). Moreover, published detection capacity of commercially

328   available antigen tests is in the range of 0.65 pg/µl (nucleocapsid protein) to 5 ng/µl (spike protein)

329   (Baker et al. 2020) (Grant et al. 2020). Thus, our chitin-based antigen detection system with a detection

330   capacity of 0.5 ng/µl fits well into the described range, suggesting that it is competitive.

331   In a next step, we envision the application of our chitin immobilization strategy for nanobodies

332   in virus detection for lateral flow assays. To date, detection of lateral flow assays is mostly enabled by

333   colloidal gold particles (Oldenburg et al. 1998 , Billingsley et al. 2017). Current investigation on chitin

334   as a building block for nanocrystals and hydrogels (Xu et al. 2020, Gu et al. 2021), as well as initial

335   experiments on drug loaded chitin scaffolds (Kovalchuk et al. 2019) demonstrates that generation of

336   colloidal chitin particles loaded with nanobodies is a future possibility to further lower antigen test

337   prices by exchanging gold as basic resource for detection by chitin.

338   Of note, we did not only verify the applicability of the nanobodies in virus detection but also

339   successfully tested the neutralization of SARS-CoV-2 *in vivo*. This confirms nanobody binding of the

340   infectious virus as opposed to only the RBD domain *in vitro*, which is necessary for antigen test

341   application. The neutralizing activity could further motivate research towards drug development using

342   unconventionally secreted proteins from *U. maydis* which as maize pathogen induces the formation of

343   edible tumors and can thus be considered innocuous for humans (Juarez-Montiel et al. 2011).

344   Nanobodies are currently discussed as novel drug targets due to ease of production, multimerization

345   and favorable *in vivo* attributes, such as improved tissue penetration and decreased immunogenicity

346   (Bannas et al. 2017, Salvador et al. 2019). Neutralizing mAbs are normally employed in

347   biopharmaceutical cocktails in patients (Marrocco et al. 2019, Sun and Ho 2020). This strategy is

348   applicable to nanobodies as well, however a study has shown comparable SARS-CoV-2 neutralization

349   between a nanobody cocktail and a bivalent version of the same nanobodies in hamster models (Pymm

350   et al. 2021), demonstrating that cocktails are not required, when bivalent constructs are used. *U. maydis*

351   might be especially suited for the generation and production of larger multivalent constructs, given its

352   ability to secrete huge proteins via the unconventional secretion route with a lack of *N*-glycosylation

353 (Stock et al. 2012). Especially, since *N*-glycosylation has been shown to negatively affect
354 pharmacokinetics of mAbs and even increased cytotoxicity before (Mastrangeli et al. 2020).

355   In summary, we provide a solid proof-of-principle for a chitin-based antigen test facilitated by
356 components derived from unconventional secretion in *U. maydis*. We envision that in combination
357 with sophisticated process engineering this technique could be developed into a lab-on-a-chip strategy
358 (Zhuang et al. 2020). Thus, protein-based immobilization of nanobodies for target capture and
359 detection are promising tools to develop alternative versatile and affordable technology for antigen
360 testing.

361

4   Materials and methods

4.1   Molecular biology methods

364   All plasmids (pUMa/pUx vectors) generated in this study were obtained using standard
365 molecular biology methods established for *U. maydis* including restriction ligation and Gibson cloning
366 (Gibson et al. 2009). Enzymes for cloning were purchased from NEB (Ipswich, MA, USA). For the
367 generation of pUMa4678 and 4679 *αgfpnb* was excised from pUMa2240 (Terfrüchte et al. 2017) by
368 hydrolyzation with BamHI and SpeI. DNA sequences encoding for Sy^{15} and Sy^{68} (Walter et al. 2020)
369 were amplified from synthetic gene blocks (IDT Coralville, IA, USA) using oligonucleotide pairs
370 oAB908/oAB909 and oAB910/oAB911, respectively (Table 1). Subsequently PCR products were
371 hydrolyzed with BamHI and SpeI and inserted into the backbone of pUMa2113 via restriction ligation
372 cloning to generate pUMa4678 and 4679. Generation of pUx4 and pUx5 was achieved by excision of
373 *αgfpnb* from pUMa2240 with BamHI and SpeI and amplification of *vhhe* and *vhhv* with BamHI and
374 SpeI restriction sites from synthetic gene blocks using oligo nucleotide pairs oCD359/oCD360 and
375 oCD363/oCD364, respectively. These sequences were subsequently hydrolyzed with BamHI and SpeI
376 and inserted into the backbone of pUMa2240 via restriction ligation cloning, thereby generating pUx4
377 and pUx5. pUx6 was generated in a similar manner. However, after the hydrolyzation of the
378 pUMa2240 backbone *vhhe* was amplified once with a BamHI and EcoRI and once with an EcoRI and
379 SpeI hydrolyzation sites. After hydrolyzation two sequences for *vhhe* were inserted into the open
380 reading frame via restriction ligation cloning, thereby encoding for fusion protein VHH[EE]-Cts1. For
381 the generation of pUx7 this process was repeated but instead of using two *vhhe* sequences with differing
382 hydrolyzation sites, the first *vhhe* sequence with BamHI and EcoRI hydrolyzation sites was exchanged
383 for *vhhv* with corresponding hydrolyzation sites.

384

385 **Table 1.** DNA oligonucleotides used in this study.

Designation	Nucleotide sequence (5´- 3´)
oMB372_jps1_fw	TTAGGCGCGCCATGCCAGGCATCTCC
oMB373_jps1_rev	TTAGGGCCCTTAGGATTCCGCATCGATTGGGG
oAB908_Sy15_fw	ATATAGGATCCATGGCGGCCCATCACCACCATCACCACCATCACCACCA TCATATGCAGGTGCAGCTCG
oAB909_Sy15_rev	ATATAACTAGTCGAGACGGTGACCTGGGTGC
oAB910_Sy68_fw	TATAGGATCCATGGCGGCCCATCACCACCATCACCACCATCACCACCAT CATATGCAGGTGCAGCTCGTCGAG
oAB911_sy68_rev	ATATATACTAGTCGAGACGGTGACCTGGGTGC
oCD359_VHH^E_fw	ATATAGGATCCATGGCGGCCCATCACCACCATCACCACCATCACCACCA TCATATGCAGGTGCAGCTCGTCG
oCD360_VHH^E_rev	ATATGAATTCATGCAGGTGCAGCTCGTCG
oCD361_VHH^E_linker	ATATACTAGTAGAGCCACCACCACCAGAGCCACCACCACCAGAGCCACC ACCACCCGACGAGACGGTGACGAGCG
oCD362_VHH^E_linker	ATATGAATTCAGAGCCACCACCACCAGAGCCACCACCACCAGAGCCACC ACCACCCGACGAGACGGTGACGAGC
oCD363_VHH^V_fw	ATATAGGATCCATGGCGGCCCATCACCACCATCACCACCATCACCACCA TCATATGCAGGTGCAGCTCGTCG
oCD364_VHH^V_rev	ATATACTAGTAGAGCCACCACCACCAGAGCCACCACCACCAGAGCCACC ACCACCCGACGAGACGGTGACCTGG
oCD365_VHH^V_linker	ATATGAATTCAGAGCCACCACCACCAGAGCCACCACCACCAGAGCCACC ACCACCCGACGAGACGGTGACCTG

386

4.2 Strain generation

388 *U. maydis* strains used in this study were obtained by homologous recombination yielding
389 genetically stable strains (Table 2). For genomic integrations at the *ip* locus, integrative plasmids were
390 used (Stock et al. 2012). For genomic integration at the *ip* locus, integrative plasmids contained the *ip*^{r}
391 allele, promoting carboxin (Cbx) resistance. Thus, plasmids were linearized within the *ip*^{r} allele using
392 restriction enzymes SspI and SwaI to allow for homologous recombination with the *ip*^{s} locus. For all
393 genetic manipulations, *U. maydis* protoplasts were transformed with linear DNA fragments. All strains
394 were verified by Southern blot analysis. For *in locus* modifications the flanking regions were amplified
395 as probes. For *ip* insertions, the probe was obtained by PCR using the primer combination
396 oMF502/oMF503 and the template pUMa260. Primer sequences are listed in Table 1.

397

398 **Table 2.** *U. maydis* strains used in this study.

Strains	Relevant genotype/ Resistance	Strain collection no. (UMa[1])	Plasmids transformed / Resistance[2]	Manipulated locus	Pro-genitor (UMa[1])	Reference
AB33P8Δ	*a2 P$_{nar}$bW2bE1* PhleoR *FRT10[um04641Δ::hyg] FRT11[um03947Δ] FRT6[um03975Δ] FRT5[um04400Δ] FRT3[um11908Δ] FRT2[um00064Δ] FRTwt[um02178Δ] FRT1[um04926Δ]* HygR	2413		*um04926*		Terfrüchte et al. 2018
AB33P8Δ Gus-Cts1	*a2 P$_{nar}$bW2bE1* PhleoR *FRT10[um04641Δ::hyg] FRT11[um03947Δ] FRT6[um03975Δ] FRT5[um04400Δ] FRT3[um11908Δ] FRT2[um00064Δ] FRTwt[um02178Δ] FRT1[um04926Δ]* HygR *ip^S[P$_{oma}$gus:shh:cts1]ip^R*CbxR	2418	pUMa2113	*ip*	2413	Terfrüchte et al. 2018
AB33P8ΔGus -Jps1	*a2 P$_{nar}$bW2bE1* PhleoR *FRT10[um04641Δ::hyg] FRT11[um03947Δ] FRT6[um03975Δ] FRT5[um04400Δ] FRT3[um11908Δ] FRT2[um00064Δ] FRTwt[um02178Δ] FRT1[um04926Δ]* HygR *ip^S[P$_{oma}$gus:shh:jps1]ip^R*CbxR	2900	pUMa3012	*ip*	2413	Philipp et al. 2022
AB33P8Δ Sy[15]-Cts1	*a2 P$_{nar}$bW2bE1* PhleoR *FRT10[um04641Δ::hyg] FRT11[um03947Δ] FRT6[um03975Δ] FRT5[um04400Δ] FRT3[um11908Δ] FRT2[um00064Δ] FRTwt[um02178Δ]*	3360	pUMa4678	*ip*	2413	This study

	$FRT1[um04926\Delta]$ HygR $ip^S[P_{oma}his:sybody\#15:ha:cts1]ip^R$CbxR					
AB33P8Δ Sy^{68}-Cts1	$a2\ P_{nar}bW2bE1$ PhleoR $FRT10[um04641\Delta::hyg]$ $FRT11[um03947\Delta]$ $FRT6[um03975\Delta]$ $FRT5[um04400\Delta]$ $FRT3[um11908\Delta]$ $FRT2[um00064\Delta]$ $FRTwt[um02178\Delta]$ $FRT1[um04926\Delta]$ HygR $ip^S[P_{oma}his:sybody\#68:ha:cts1]ip^R$CbxR	3361	pUMa4679	*ip*	2413	This study
AB33P8Δ Sy$^{68/15}$-Cts1	$a2\ P_{nar}bW2bE1$ PhleoR $FRT10[um04641\Delta::hyg]$ $FRT11[um03947\Delta]$ $FRT6[um03975\Delta]$ $FRT5[um04400\Delta]$ $FRT3[um11908\Delta]$ $FRT2[um00064\Delta]$ $FRTwt[um02178\Delta]$ $FRT1[um04926\Delta]$ HygR $ip^S[P_{oma}sybody\#68:his:sybody\#15:ha:cts1]ip^R$CbxR	Ux1	pUx1	*ip*	2413	Philipp et al. 2022
AB33P8Δ VHH^E-Cts1	$a2\ P_{nar}bW2bE1$ PhleoR $FRT10[um04641\Delta::hyg]$ $FRT11[um03947\Delta]$ $FRT6[um03975\Delta]$ $FRT5[um04400\Delta]$ $FRT3[um11908\Delta]$ $FRT2[um00064\Delta]$ $FRTwt[um02178\Delta]$ $FRT1[um04926\Delta]$ HygR $ip^S[P_{oma}his:vhhe:gs:ha:cts1]ip^R$CbxR	Ux4	pUx4	*ip*	2413	This study
AB33P8Δ VHH^V-Cts1	$a2\ P_{nar}bW2bE1$ PhleoR $FRT10[um04641\Delta::hyg]$ $FRT11[um03947\Delta]$ $FRT6[um03975\Delta]$ $FRT5[um04400\Delta]$ $FRT3[um11908\Delta]$ $FRT2[um00064\Delta]$ $FRTwt[um02178\Delta]$	Ux5	pUx5	*ip*	2413	This study

	$FRT1[um04926\Delta]$ HygR $ip^S[P_{oma}his:vhhv:gs:ha:cts1]ip^R$CbxR					
AB33P8Δ VHH^{EE}-Cts1	$a2\ P_{nar}bW2bE1$ PhleoR $FRT10[um04641\Delta::hyg]$ $FRT11[um03947\Delta]$ $FRT6[um03975\Delta]$ $FRT5[um04400\Delta]$ $FRT3[um11908\Delta]$ $FRT2[um00064\Delta]$ $FRTwt[um02178\Delta]$ $FRT1[um04926\Delta]$ HygR $ip^S[P_{oma}his:vhhe:gs:vhhe:gs:ha:cts1]ip^R$CbxR	Ux6	pUx6	ip	2413	This study
AB33P8Δ VHH^{VE}-Cts1	$a2\ P_{nar}bW2bE1$ PhleoR $FRT10[um04641\Delta::hyg]$ $FRT11[um03947\Delta]$ $FRT6[um03975\Delta]$ $FRT5[um04400\Delta]$ $FRT3[um11908\Delta]$ $FRT2[um00064\Delta]$ $FRTwt[um02178\Delta]$ $FRT1[um04926\Delta]$ HygR $ip^S[P_{oma}his:vhhv:gs:vhhe:gs:ha:cts1]ip^R$CbxR	Ux7	pUx7	ip	2413	This study
AB33P8Δ Sy$^{68/15}$-Jps1	$a2\ P_{nar}bW2bE1$ PhleoR $FRT10[um04641\Delta::hyg]$ $FRT11[um03947\Delta]$ $FRT6[um03975\Delta]$ $FRT5[um04400\Delta]$ $FRT3[um11908\Delta]$ $FRT2[um00064\Delta]$ $FRTwt[um02178\Delta]$ $FRT1[um04926\Delta]$ HygR $ip^S[P_{oma}sybody\#68:his:sybody\#15:ha:jps1]ip^R$ CbxR	Ux8	pUx8	ip	2413	Philipp et al. 2022

399 ^{1} Internal strain collection numbers (UMa/Ux codes)

400 ^{2} Plasmids generated in our working group are integrated in a plasmid collection and termed pUMa or pUx plus a 4-digit

401 number as identifier.

402

403 **4.3 Cultivation**

404   *U. maydis* strains were grown at 28 °C in complete medium supplemented with 1% (w/v) glucose

405   (CM-glc) if not described differently. Solid media were supplemented with 2% (w/v) agar agar. Growth

406   phenotypes were evaluated using the BioLector microbioreactor (m2p-labs). MTP-R48-BOH round

407   plates were inoculated with 1.5 ml culture per well and incubated at 1,000 rpm at 28 °C. Backscatter

408   light with a gain of 25 or 20 was used to determine biomass.

409

4.4   Quantification of Gus activity on chitin beads

411   Gus activity was determined to quantify chitin binding of Gus-Cts1 using the specific substrate

412   4-methylumbelliferyl β-D galactopyranoside (MUG, Sigma–Aldrich). To his end 50 µg of *U. maydis*

413   cell extracts were diluted in chitin binding buffer to a final volume of 500 µl. 50 µl chitin magnetic

414   beads (New England Biolabs, Ipswich, MA, USA) were washed with 500 µl water, equilibrated with

415   500 µl chitin binding buffer (500 mM NaCl, 50 mM Tris-HCl buffer pH 8.0, 0,05 % Tween-20 (v/v))

416   and subsequently incubated with cell extracts in binding buffer at 4 °C on a stirring wheel for 16 h.

417   Subsequently, chitin beads were washed with 500 µl chitin binding buffer and 500 µl of water, taken

418   up in 2✕ Gus assay buffer (10 mM sodium phosphate buffer pH 7.0, 28 µM β-mercaptoethanol, 0.8

419   mM EDTA, 0.0042% (v/v) lauroyl-sarcosin, 0.004% (v/v) Triton X-100, 2 mM MUG, 0.2 mg/ml (w/v)

420   BSA) and transferred to black 96-well plates. Relative fluorescence units (RFUs) were determined

421   using a plate reader (Tecan, Männedorf, Switzerland) for 100 min at 28 °C with measurements every

422   5 minutes (excitation/emission wavelengths: 365/465 nm, gain 60). For quantification of conversion

423   of MUG to the fluorescent product 4-methylumbelliferone (MU), a calibration curve was determined

424   using 0, 1, 5, 10, 25, 50, 100, 200 µM MU.

425

4.5   Trichloroacetic acid precipitation

427   Gus-Cts1 and Gus-Jps1 secretion was analyzed by TCA precipitation of culture broths.

428   Therefore, 2 ml of cultures grown in Verduyn medium (55.5 mM Glucose, 74.7 mM NH_4Cl, 0.81 mM

429       $MgSO_4$✕$7H_2O$, 0.036 mM $FeSO_4\times7H_2O$, 36.7 mM KH_2PO_4, 100 mM MES pH 6.5, 0.051 mM EDTA,

430   0.025 mM $ZnSO_4$✕$7H_2O$, 0.041 mM $CaCl_2$, 0.016 mM H_3bBO_3, 6.7 µM $MnCl_2\times2H_2O$, 2.3 µM

431       $CoCl_2\times6H_2O$, 1.9 µM $CuSO_4\times5H_2O$, 1.9 µM Na_2MoO_4✕$2H_2O$, 0.6 µM KI) to an OD_{600} of 3 were

432   harvested by centrifugation at $11.000 \times g$ and supernatant was transferred to a fresh reaction tube. 1

433   ml of cell free supernatants of cultures were chilled on ice, mixed with 400 µl 50% (v/v) TCA solution

434   and incubated on ice at 4 °C overnight. Subsequently, protein pellets were harvested by centrifugation

435   at 11.000 **×** g at 4 °C for 30 min. Supernatants were discarded and pellets were washed with 300 µl of

436   -20 °C acetone followed by centrifugation at 11.000 × g at 4 °C for 20 min two times. Pellets were

437   dried at room temperature and resuspended in Laemmli buffer containing 0.12 M NaOH. Resuspended

438   pellets were denatured at 95 °C for 10 min and then subjected to SDS-PAGE and Western blot analysis.

439

4.6   Generation of cell extracts

441   For the verification of protein production via Western blot or further IMAC purification, cultures

442   were grown to an OD_{600} of 1.0 and harvested at $5000 \times g$ for 5 min in centrifugation tubes. Until further

443   use, pellets were stored at -20 °C. For preparation of cell extracts, cell pellets were resuspended in 1

444   ml cell extract lysis buffer (100 mM sodium phosphate buffer pH 8.0, 10 mM Tris/HCl pH 8.0, 8 M

445   urea, 1 mM DTT, 1 mM PMSF, 2.5 mM benzamidine, 1 mM pepstatin A, 2× complete protease

446   inhibitor cocktail (Roche, Sigma/Aldrich, Billerica, MA, United States) and cells were crushed by

447   agitation with glass beads at 2,500 rpm for 12 min at 4 °C. After centrifugation ($11,000 \times g$ for 30 min

448   at 4°C), the supernatant was separated from cell debris and was transferred to a fresh reaction tube. For

449   direct use protein concentration was determined by Bradford assay (BioRad, Hercules, CA, United

450   States) (Bradford 1976). Otherwise, cell extracts were subjected to IMAC purification.

451

4.7 SDS PAGE and Western blot analysis

453   To assay protein production and secretion, 10 µg of cell extract or TCA precipitated samples

454   were subjected to SDS-PAGE. SDS-PAGE was conducted using 10% (w/v) acrylamide gels.

455   Subsequently, proteins were transferred to methanol activated PVDF membranes using semi-dry

456   Western blotting. Nanobody fusion proteins were detected using a primary anti-HA (mouse; 1:3,000,

457   Sigma-Aldrich, St. Louis, MO, USA). An anti-mouse IgG-horseradish peroxidase (HRP) conjugate

458   (1:3,000 Promega, Fitchburg, United States) was used as secondary antibody. HRP activity was

459   detected using the Amersham ™ ECL ™ Prime Western Blotting Detection Reagent (GE Healthcare,

460   Chalfont St Giles, United Kingdom) and a LAS4000 chemiluminescence imager (GE Healthcare Life

461   Sciences, Freiburg, Germany).

462

4.8 IMAC purification of His-tagged protein

464   Purification of *U. maydis* derived nanobody fusion proteins was achieved by generation of cell

465   extracts from 400 ml of *U. maydis* culture harvested at an OD_{600} of 1.0 and subsequent Nickel^{2+}-NTA

466   purification. Therefore, culture harvested at 5000 ✖ g for 5 min was resuspended in 8 ml lysis buffer

467   (10 mM imidazole, 50 mM NaH_2PO_4, 300 mM NaCl, pH 8.0), 1.6 ml glass beads were added to cell

468   suspension and cells were crushed by agitation with glass beads at 2,500 rpm at 4 °C for 12 min.

469   Subsequently, cell debris was removed by centrifugation at 11,000 ✖ g at 4 °C for 30 min. Nickel^{2+}-

470   NTA matrix was settled in empty columns and after flow-through of ethanol, equilibrated with 10

471   column volumes of lysis buffer. Subsequently, matrix was dissolved in cleared cell extracts and the

472   mixture was incubated on a stirring wheel at 4 °C for 1 h. Subsequently, flow-through was discarded

473   and matrix was washed with 5 column volumes of washing buffer (20 mM imidazole 50 mM NaH_2PO_4,

474   300 mM NaCl, pH 8.0). Protein was eluted in two fractions of 2 ml each using elution buffer 1 (lysis

475   buffer, 150 mM imidazole) and elution buffer 2 (lysis buffer, 250 mM imidazole). For application in

476   ELISA elution fractions were pooled via Amicon Ultra-15 50k centrifugal filter units (Merck Millipore,

477   Burlington, MA, USA). Elution buffer was chosen for the intended application (coating buffer for

478   sandwich ELISA, chitin binding buffer for chitin ELISA, PBS-T for direct detection, see chapters 4.10-

479   4.11 for buffer composition).

480

4.9 *In vivo* neutralization assays

482   Nanobodies were IMAC purified and stored at 4 °C prior to incubation with SARS-CoV-2.

483   Nanobodies at concentration of 0.5 mg/ml in PBS-buffer were incubated with SARS-CoV-2 particles

484   in serial dilutions for 1 h at 37 °C. Subsequently, Vero cells (ATCC-CCL-81) displaying ACE2 were

485   inoculated with pre incubated samples. After three days of incubation visual microscopic analysis was

486   conducted using an Eclipse TS100 (Nikon, Minato, Japan) to observe cytopathic effects and thus

487   determine if infection had occurred. qPCR analysis was conducted using anti-SARS-CoV-2 primer

488   pairs specific to the E-gene (Corman et al. 2020) and Lightmix Modular SARS and Wuhan CoV E-

489   gene (Roche Lifescience, Basel, Switzerland) in an ABI 7500 Fast PCR cycler (PE applied biosystems,

490   Waltham, MA, USA).

4.10 Direct ELISA

492   For detection of nanobody binding activity protein adsorbing 384-well microtiter plates

493   (Nunc® Maxisorp™, ThermoFisher Scientific, Waltham, MA, USA) were used. Wells were coated

494   with 1 µg Gfp for anti-GfpNB or 1 µg commercially available SARS-CoV-2 Spike-RBD-domain

495   protein for SARS-CoV-2 nanobody-Cts1-fusion proteins (Invitrogen, Waltham Massachusetts, USA).

496   Recombinant Gfp was produced in *E. coli* and purified by Ni^{2+}-chelate affinity chromatography as

497   described earlier (Terfrüchte et al. 2017). 1 µg BSA per well dealt as negative control (NEB, Ipswich,

498   MA, USA). Samples were applied in a final volume of 100 µl coating buffer (100 mM Tris-HCL pH

499   8, 150 mM NaCl, 1 mM EDTA) per well at room temperature for at least 16 h. Blocking was conducted

500   for at least 4 h at room temperature with 5% (w/v) skimmed milk in coating buffer. Subsequently, 5%

501   (w/v) skimmed milk in PBS (137 mM NaCl, 2.7 mM KCl, 10 mM Na_2HPO_4, 1.8 mM KH_2PO_4, pH

502   7.2) were added to defined protein amounts of nanobody fusion protein samples purified from culture

503   supernatants or cell extracts via Ni^{2+}-NTA gravity flow and respective controls. 100 µl of sample was

504   added to wells coated with the cognate antigen and BSA. The plate was incubated with samples and

505   controls over night at 4 °C. After 3✕ PBS-T (PBS supplemented with 0.05% (v/v) Tween-20, 100 µl

506   per well) washing, a primary anti-HA antibody (mouse, Sigma-Aldrich, St. Louis, MO, USA) 1: 5,000

507   diluted in PBS supplemented with skimmed milk (5% w/v) was added (100 µl per well) and incubated

508   for 2 h at room temperature. Then wells were washed again three times with PBS-T (100 µl per well)

509   and incubated with a secondary mouse-HRP antibody (goat, Promega, Madison, WI, USA) (50 µl per

510   well) for 1 h at room temperature (1: 5,000 in PBS supplemented with skimmed milk (5% w/v)).

511   Subsequently, wells were washed three times with PBS-T and three times with PBS and incubated with

512   Quanta Red™ enhanced chemifluorescent HRP substrate (50:50:1, 50 µl per well, ThermoFisher

513   Scientific, Waltham, MA, USA) at room temperature for 15 min. The reaction was stopped with 10 µl

514   Quanta Red™ stop solution per well and fluorescence readout was performed at 570 nm excitation and

515   600 nm emission using an Infinite M200 plate reader (Tecan, Männedorf, Switzerland).

516   For ELISA against the full-length spike protein, experiments were carried out with the Anti-SARS-

517   CoV-2-QuantiVac-ELISA (IgG)-Kit (Euroimmun, Lübeck, Germany) according to the manual.

518   Controls were detected using the secondary anti-human-HRP antibody delivered with the Kit.

519   Nanobody fusions were detected using anti-HA-HRP (Miltenyi Biotec, Bergisch Gladbach, Germany).

520

521   **4.11 Sandwich ELISA**

522   To determine nanobody-Cts1-fusion capabilities to act as capture antibody for an antigen test

523   application, a mixture of 0.5 µg of IMAC purified protein and 0.5 µg BSA (New England Biolabs,

524   Ipswich, MA, USA) in 100 µl of coating buffer per well was added to 384-well microtiter plates (1 µg

525   without BSA for direct detection). Coating was conducted for 16 h at 4 °C. Subsequently, plates were

526   blocked with 5% skimmed milk in coating buffer for 2 h at room temperature. RBD samples were

527   added in serial dilutions in a volume of 100 µl sample buffer (5% skimmed milk powder in PBS-T)

528   and incubated for 2 h at room temperature. Subsequently plates were washed 3 times with PBS-T and

529   primary antibody (anti-RBD-mouse, R&D systems, Minneapolis, MN, USA) was added in a dilution

530   of 1: 5,000 in sample buffer and incubated for 2 h at room temperature. Afterwards wells were washed

531   again with PBS-T thrice and incubated with secondary mouse-HRP antibody (goat, Promega,

532   Fitchburg, WI, United States) was added in a dilution of 1: 5,000 in 50 µl sample buffer and incubated

533   for 1 h at room temperature. Prior to detection plates were washed thrice with 100 µl PBS-T and three

534   times with 100 µl PBS per well. Detection was carried out using Quanta Red™ enhanced

535   chemifluorescent HRP substrate (50:50:1, 50 µl per well, ThermoFisher Scientific, Waltham, MA,

536   USA) at room temperature for 10 min. The reaction was stopped with 10 µl Quanta Red™ stop solution

537   per well and fluorescence readout was performed at 570 nm excitation and 600 nm emission using an

538   Infinite M200 plate reader (Tecan, Männedorf, Switzerland).

539

4.12 Chitin based sandwich ELISA

541   For chitin-based sandwich ELISA 50 µl of chitin magnetic beads (New England Biolabs,

542   Ipswich, MA, USA) were transferred into a 1.5 ml reaction tube, washed with 500 µl of water and

543   equilibrated in 500 µl of chitin binding buffer (500 mM NaCl, 50 mM Tris-HCl buffer pH 8.0, 0,05%

544   Tween-20 (v/v)). Subsequently 2 µg of IMAC purified protein was added in a final volume of 500 µl

545   chitin binding buffer. Coating was conducted on a stirring wheel at 4 °C for 16 h. Afterwards chitin

546   beads were blocked with 5% skimmed milk powder in chitin binding buffer on a stirring wheel at room

547   temperature for 2 h. In the next step chitin beads were washed thrice with PBS-T, RBD samples were

548   added in serial dilutions in a volume of 100 µl ELISA sample buffer and incubated on a stirring wheel

549   at room temperature for 2 h. After removal of the sample buffer chitin magnetic beads were taken up

550   in 100 µl PBS-T, transferred to a fresh reaction tube and subsequently washed three times with 500 µl

551   PBS-T before addition of primary antibody (R&D systems, Minneapolis, MN, USA) 1:5000 in 200 µl

552   sample buffer. The primary antibody was incubated with chitin magnetic beads on a stirring wheel at

553   room temperature for 2 h. Subsequent to primary antibody removal chitin magnetic beads were washed

554   three times with PBS-T and incubated with secondary mouse-HRP antibody (goat, Promega, Fitchburg,

555   United States) 1:5000 in 100 µl sample buffer on a stirring wheel at room temperature for 1 h. For

556   detection chitin magnetic beads were washed three times with 500 µl PBS-T and three times with 500

557   µl PBS before being taken up in 100 µl Quanta Red™ enhanced chemifluorescent HRP substrate

558   (50:50:1, 50 µl per well, ThermoFisher Scientific, Waltham, MA, USA) and transferred to a black 96-

559 well microtiter plate. Fluorescence readout was performed 2 min after addition of the substrate at 570

560 nm excitation and 600 nm emission using an Infinte M200 plate reader (Tecan, Männedorf,

561 Switzerland) after stopping of the reaction with 10 µl QuantaRed™ stop solution.

562 **5 Author contributions**

563 M.P., L.M, M.A. and K.P.H designed the experiments. K.P.H. conducted initial chitin binding

564 experiments (Fig. 3 B). L.M. conducted neutralization experiments and RT-PCR (Fig. 2). M.A.

565 conducted direct ELISA against full length S1 (Fig. 1 D) M.P. purified nanobodies for neutralization

566 experiments and direct S1-ELISA and conducted all other experiments. M.P. designed and prepared

567 the figures and tables. K.S., H.S. and M.F. supervised the project. M.P. prepared the manuscript with

568 advice from K.S.

569

570 **6 Funding**

577

578 **7 Acknowledgements**

580

581

582

583

584

585

586

587

588

589

8 References

Andryukov BG. (2020). Six decades of lateral flow immunoassay: from determining metabolic markers to diagnosing COVID-19. *AIMS Microbiol*.**6**:280-304. Epub 20200826 DOI: 10.3934/microbiol.2020018

Baker AN, Richards SJ, Guy CS, Congdon TR, Hasan M, Zwetsloot AJ, Gallo A, Lewandowski JR, Stansfeld PJ, Straube A, et al. (2020). The SARS-COV-2 Spike Protein Binds Sialic Acids and Enables Rapid Detection in a Lateral Flow Point of Care Diagnostic Device. *ACS Cent Sci*. Nov 25;**6**:2046-2052. Epub 20200923 DOI: 10.1021/acscentsci.0c00855

Bannas P, Hambach J, Koch-Nolte F. (2017). Nanobodies and Nanobody-Based Human Heavy Chain Antibodies As Antitumor Therapeutics. *Front Immunol*.**8**:1603. Epub 20171122 DOI: 10.3389/fimmu.2017.01603

Baral P, Bhattarai N, Hossen ML, Stebliankin V, Gerstman BS, Narasimhan G, Chapagain PP. (2021). Mutation-induced changes in the receptor-binding interface of the SARS-CoV-2 Delta variant B.1.617.2 and implications for immune evasion. *Biochem Biophys Res Commun*. Oct 15;**574**:14-19. Epub 20210815 DOI: 10.1016/j.bbrc.2021.08.036

Bierle DM, Ganesh R, Razonable RR. (2021). Breakthrough COVID-19 and casirivimab-imdevimab treatment during a SARS-CoV-2 B1.617.2 (Delta) surge. *J Clin Virol*. Dec;**145**:105026. Epub 20211108 DOI: 10.1016/j.jcv.2021.105026

Billingsley MM, Riley RS, Day ES. (2017). Antibody-nanoparticle conjugates to enhance the sensitivity of ELISA-based detection methods. *PLoS One*.**12**:e0177592. Epub 20170511 DOI: 10.1371/journal.pone.0177592

Callaway E. (2020). COVID vaccine excitement builds as Moderna reports third positive result. *Nature*. Nov;**587**:337-338 DOI: 10.1038/d41586-020-03248-7

Chong S, Mersha FB, Comb DG, Scott ME, Landry D, Vence LM, Perler FB, Benner J, Kucera RB, Hirvonen CA, et al. (1997). Single-column purification of free recombinant proteins using a self-cleavable affinity tag derived from a protein splicing element. *Gene*. Jun 19;**192**:271-281 DOI: 10.1016/s0378-1119(97)00105-4

Chong S, Williams KS, Wotkowicz C, Xu MQ. (1998). Modulation of protein splicing of the Saccharomyces cerevisiae vacuolar membrane ATPase intein. *J Biol Chem*. Apr 24;**273**:10567-10577 DOI: 10.1074/jbc.273.17.10567

Corman VM, Landt O, Kaiser M, Molenkamp R, Meijer A, Chu DK, Bleicker T, Brunink S, Schneider J, Schmidt ML, et al. (2020). Detection of 2019 novel coronavirus (2019-nCoV) by real-time RT-PCR. *Euro Surveill*. Jan;**25** DOI: 10.2807/1560-7917.ES.2020.25.3.2000045

Custodio TF, Das H, Sheward DJ, Hanke L, Pazicky S, Pieprzyk J, Sorgenfrei M, Schroer MA, Gruzinov AY, Jeffries CM, et al. (2020). Selection, biophysical and structural analysis of synthetic nanobodies that effectively neutralize SARS-CoV-2. *Nat Commun*. Nov 4;**11**:5588. Epub 20201104 DOI: 10.1038/s41467-020-19204-y

Fernandes CS, Dos Santos R, Ottengy S, Viecinski AC, Behar G, Mouratou B, Pecorari F, Roque AC. (2016). Affitins for protein purification by affinity magnetic fishing. *J Chromatogr A*. Jul 29;**1457**:50-58. Epub 20160607 DOI: 10.1016/j.chroma.2016.06.020

Fernandes Q, Inchakalody VP, Merhi M, Mestiri S, Taib N, Moustafa Abo El-Ella D, Bedhiafi T, Raza A, Al-Zaidan L, Mohsen MO, et al. (2022). Emerging COVID-19 variants and their

632   impact on SARS-CoV-2 diagnosis, therapeutics and vaccines. *Ann Med*. Dec;**54**:524-540 DOI:
633   10.1080/07853890.2022.2031274

634 **Field J, Nikawa J, Broek D, MacDonald B, Rodgers L, Wilson IA, Lerner RA, Wigler M**. (1988).
635   Purification of a RAS-responsive adenylyl cyclase complex from Saccharomyces cerevisiae by
636   use of an epitope addition method. *Mol Cell Biol*. May;**8**:2159-2165   DOI:
637   10.1128/mcb.8.5.2159-2165.1988

638 **Fleissner A, Dersch P**. (2010). Expression and export: recombinant protein production systems for
639   Aspergillus. *Appl Microbiol Biotechnol*. Jul;**87**:1255-1270. Epub 2010/06/10   DOI:
640   10.1007/s00253-010-2672-6

641 **Franzreb M, Siemann-Herzberg M, Hobley TJ, Thomas OR**. (2006). Protein purification using
642   magnetic adsorbent particles. *Appl Microbiol Biotechnol*. May;**70**:505-516. Epub 20060223
643   DOI: 10.1007/s00253-006-0344-3

644 **Gauhar A, Privezentzev CV, Demydchuk M, Gerlza T, Rieger J, Kungl AJ, Walsh FS, Rutkowski
645   JL, Stocki P**. (2021). Single domain shark VNAR antibodies neutralize SARS-CoV-2 infection
646   in vitro. *FASEB J*. Nov;**35**:e21970 DOI: 10.1096/fj.202100986RR

647 **Gibson DG, Young L, Chuang RY, Venter JC, Hutchison CA, 3rd, Smith HO**. (2009). Enzymatic
648   assembly of DNA molecules up to several hundred kilobases. *Nat Methods*. May;**6**:343-345.
649   Epub 2009/04/14 DOI: 10.1038/nmeth.1318

650 **Grant BD, Anderson CE, Williford JR, Alonzo LF, Glukhova VA, Boyle DS, Weigl BH, Nichols
651   KP**. (2020). SARS-CoV-2 Coronavirus Nucleocapsid Antigen-Detecting Half-Strip Lateral
652   Flow Assay Toward the Development of Point of Care Tests Using Commercially Available
653   Reagents. *Anal Chem*. Aug 18;**92**:11305-11309. Epub 20200805   DOI:
654   10.1021/acs.analchem.0c01975

655 **Gu S, Tian Y, Liang K, Ji Y**. (2021). Chitin nanocrystals assisted 3D printing of polycitrate thermoset
656   bioelastomers. *Carbohydr Polym*. Mar 15;**256**:117549. Epub 20201220   DOI:
657   10.1016/j.carbpol.2020.117549

658 **Guerrero F, Ciragan A, Iwai H**. (2015). Tandem SUMO fusion vectors for improving soluble protein
659   expression and purification. *Protein Expr Purif*. Dec;**116**:42-49. Epub 20150820 DOI:
660   10.1016/j.pep.2015.08.019

661 **Hulswit RJ, de Haan CA, Bosch BJ**. (2016). Coronavirus Spike Protein and Tropism Changes. *Adv
662   Virus Res*.**96**:29-57. Epub 20160913 DOI: 10.1016/bs.aivir.2016.08.004

663 **Huo J, Le Bas A, Ruza RR, Duyvesteyn HME, Mikolajek H, Malinauskas T, Tan TK, Rijal P,
664   Dumoux M, Ward PN, et al.** (2020). Neutralizing nanobodies bind SARS-CoV-2 spike RBD
665   and block interaction with ACE2. *Nat Struct Mol Biol*. Sep;**27**:846-854. Epub 20200713 DOI:
666   10.1038/s41594-020-0469-6

667 **Jain J, Gaur S, Chaudhary Y, Kaul R**. (2020). The molecular biology of intracellular events during
668   Coronavirus infection cycle. *Virusdisease*. Jun;**31**:75-79. Epub 20200504   DOI:
669   10.1007/s13337-020-00591-1

670 **Juarez-Montiel M, Ruiloba de Leon S, Chavez-Camarillo G, Hernandez-Rodriguez C, Villa-
671   Tanaca L**. (2011). Huitlacoche (corn smut), caused by the phytopathogenic fungus Ustilago
672   maydis, as a functional food. *Rev Iberoam Micol*. Apr-Jun;**28**:69-73. Epub 20110223 DOI:
673   10.1016/j.riam.2011.01.001

674 **Kirchdoerfer RN, Cottrell CA, Wang N, Pallesen J, Yassine HM, Turner HL, Corbett KS,**
675 **Graham BS, McLellan JS, Ward AB**. (2016). Pre-fusion structure of a human coronavirus
676 spike protein. *Nature*. Mar 3;**531**:118-121 DOI: 10.1038/nature17200

677 **Ko H, Kang M, Kim MJ, Yi J, Kang J, Bae JH, Sohn JH, Sung BH**. (2021). A novel protein fusion
678 partner, carbohydrate-binding module family 66, to enhance heterologous protein expression
679 in Escherichia coli. *Microb Cell Fact*. Dec 28;**20**:232. Epub 20211228 DOI: 10.1186/s12934-
680 021-01725-w

681 **König PA, Das H, Liu H, Kummerer BM, Gohr FN, Jenster LM, Schiffelers LDJ, Tesfamariam**
682 **YM, Uchima M, Wuerth JD, et al.** (2021). Structure-guided multivalent nanobodies block
683 SARS-CoV-2 infection and suppress mutational escape. *Science*. Feb 12;**371**. Epub 2021/01/14
684 DOI: 10.1126/science.abe6230

685 **Korber B, Fischer WM, Gnanakaran S, Yoon H, Theiler J, Abfalterer W, Hengartner N, Giorgi**
686 **EE, Bhattacharya T, Foley B, et al.** (2020). Tracking Changes in SARS-CoV-2 Spike:
687 Evidence that D614G Increases Infectivity of the COVID-19 Virus. *Cell*. Aug 20;**182**:812-827
688 e819. Epub 20200703 DOI: 10.1016/j.cell.2020.06.043

689 **Kovalchuk V, Voronkina A, Binnewerg B, Schubert M, Muzychka L, Wysokowski M, Tsurkan**
690 **MV, Bechmann N, Petrenko I, Fursov A, et al.** (2019). Naturally Drug-Loaded Chitin:
691 Isolation and Applications. *Mar Drugs*. Oct 10;**17**. Epub 20191010 DOI:
692 10.3390/md17100574

693 **Kudlay D, Svistunov A**. (2022). COVID-19 Vaccines: An Overview of Different Platforms.
694 *Bioengineering (Basel)*. Feb 12;**9**. Epub 20220212 DOI: 10.3390/bioengineering9020072

695 **Li W, Moore MJ, Vasilieva N, Sui J, Wong SK, Berne MA, Somasundaran M, Sullivan JL,**
696 **Luzuriaga K, Greenough TC, et al.** (2003). Angiotensin-converting enzyme 2 is a functional
697 receptor for the SARS coronavirus. *Nature*. Nov 27;**426**:450-454 DOI: 10.1038/nature02145

698 **Lin AV**. (2015). Direct ELISA. *Methods Mol Biol*.**1318**:61-67 DOI: 10.1007/978-1-4939-2742-5_6

699 **Marrocco I, Romaniello D, Yarden Y**. (2019). Cancer Immunotherapy: The Dawn of Antibody
700 Cocktails. *Methods Mol Biol*.**1904**:11-51 DOI: 10.1007/978-1-4939-8958-4_2

701 **Mastrangeli R, Audino MC, Palinsky W, Broly H, Bierau H**. (2020). The Formidable Challenge of
702 Controlling High Mannose-Type N-Glycans in Therapeutic mAbs. *Trends Biotechnol*.
703 Oct;**38**:1154-1168. Epub 20200629 DOI: 10.1016/j.tibtech.2020.05.009

704 **Matusali G, Colavita F, Lapa D, Meschi S, Bordi L, Piselli P, Gagliardini R, Corpolongo A,**
705 **Nicastri E, Antinori A, et al.** (2021). SARS-CoV-2 Serum Neutralization Assay: A Traditional
706 Tool for a Brand-New Virus. *Viruses*. Apr 10;**13**. Epub 20210410 DOI: 10.3390/v13040655

707 **Müller L, Ostermann PN, Walker A, Wienemann T, Mertens A, Adams O, Andree M, Hauka S,**
708 **Lubke N, Keitel V, et al.** (2021). Sensitivity of anti-SARS-CoV-2 serological assays in a high-
709 prevalence setting. *Eur J Clin Microbiol Infect Dis*. May;**40**:1063-1071. Epub 20210203 DOI:
710 10.1007/s10096-021-04169-7

711 **Muyldermans S**. (2013). Nanobodies: natural single-domain antibodies. *Annu Rev Biochem*.**82**:775-
712 797. Epub 2013/03/19 DOI: 10.1146/annurev-biochem-063011-092449

713 **Muyldermans S, Baral TN, Retamozzo VC, De Baetselier P, De Genst E, Kinne J, Leonhardt H,**
714 **Magez S, Nguyen VK, Revets H, et al.** (2009). Camelid immunoglobulins and nanobody
715 technology. *Vet Immunol Immunopathol*. Mar 15;**128**:178-183. Epub 20081017 DOI:
716 10.1016/j.vetimm.2008.10.299

717 **Oldenburg SJ, Averitt RD, Westcott SL, Halas NJ**. (1998). Nanoengineering of optical resonances.
718   *Chemical Physics Letters*.**288**:234-247

719 **Ou X, Liu Y, Lei X, Li P, Mi D, Ren L, Guo L, Guo R, Chen T, Hu J, et al.** (2020). Characterization
720   of spike glycoprotein of SARS-CoV-2 on virus entry and its immune cross-reactivity with
721   SARS-CoV. *Nat Commun*. Mar 27;**11**:1620. Epub 20200327 DOI: 10.1038/s41467-020-
722   15562-9

723 **Philipp M, Hussnaetter KP, Reindl M, Muntjes K, Feldbrugge M, Schipper K**. (2021). A Novel
724   Potent Carrier for Unconventional Protein Export in Ustilago maydis. *Front Cell Dev*
725   *Biol*.**9**:816335. Epub 20220110 DOI: 10.3389/fcell.2021.816335

726 **Porath J, Carlsson J, Olsson I, Belfrage G**. (1975). Metal chelate affinity chromatography, a new
727   approach to protein fractionation. *Nature*. Dec 18;**258**:598-599 DOI: 10.1038/258598a0

728 **Pymm P, Adair A, Chan LJ, Cooney JP, Mordant FL, Allison CC, Lopez E, Haycroft ER, O'Neill**
729   **MT, Tan LL, et al.** (2021). Nanobody cocktails potently neutralize SARS-CoV-2 D614G
730   N501Y variant and protect mice. *Proc Natl Acad Sci U S A*. May 11;**118** DOI:
731   10.1073/pnas.2101918118

732 **Reindl M, Hansch S, Weidtkamp-Peters S, Schipper K**. (2019). A Potential Lock-Type Mechanism
733   for Unconventional Secretion in Fungi. *Int J Mol Sci*. Jan 22;**20**. Epub 2019/01/27 DOI:
734   10.3390/ijms20030460

735 **Reindl M, Stock J, Hussnaetter KP, Genc A, Brachmann A, Schipper K**. (2020). A Novel Factor
736   Essential for Unconventional Secretion of Chitinase Cts1. *Front Microbiol*.**11**:1529. Epub
737   2020/08/01 DOI: 10.3389/fmicb.2020.01529

738 **Salvador JP, Vilaplana L, Marco MP**. (2019). Nanobody: outstanding features for diagnostic and
739   therapeutic applications. *Anal Bioanal Chem*. Mar;**411**:1703-1713. Epub 20190208 DOI:
740   10.1007/s00216-019-01633-4

741 **Santos RD, Iria I, Manuel AM, Leandro AP, Madeira CAC, Goncalves J, Carvalho AL, Roque**
742   **ACA**. (2020). Magnetic Precipitation: A New Platform for Protein Purification. *Biotechnol J*.
743   Sep;**15**:e2000151. Epub 20200708 DOI: 10.1002/biot.202000151

744 **Sarkari P, Reindl M, Stock J, Müller O, Kahmann R, Feldbrugge M, Schipper K**. (2014).
745   Improved expression of single-chain antibodies in Ustilago maydis. *J Biotechnol*. Dec
746   10;**191**:165-175. Epub 2014/07/06 DOI: 10.1016/j.jbiotec.2014.06.028

747 **Stock J, Sarkari P, Kreibich S, Brefort T, Feldbrugge M, Schipper K**. (2012). Applying
748   unconventional secretion of the endochitinase Cts1 to export heterologous proteins in Ustilago
749   maydis. *J Biotechnol*. Oct 15;**161**:80-91. Epub 2012/03/27 DOI: 10.1016/j.jbiotec.2012.03.004

750 **Stock J, Terfruchte M, Schipper K**. (2016). A Reporter System to Study Unconventional Secretion
751   of Proteins Avoiding N-Glycosylation in Ustilago maydis. *Methods Mol Biol*.**1459**:149-160.
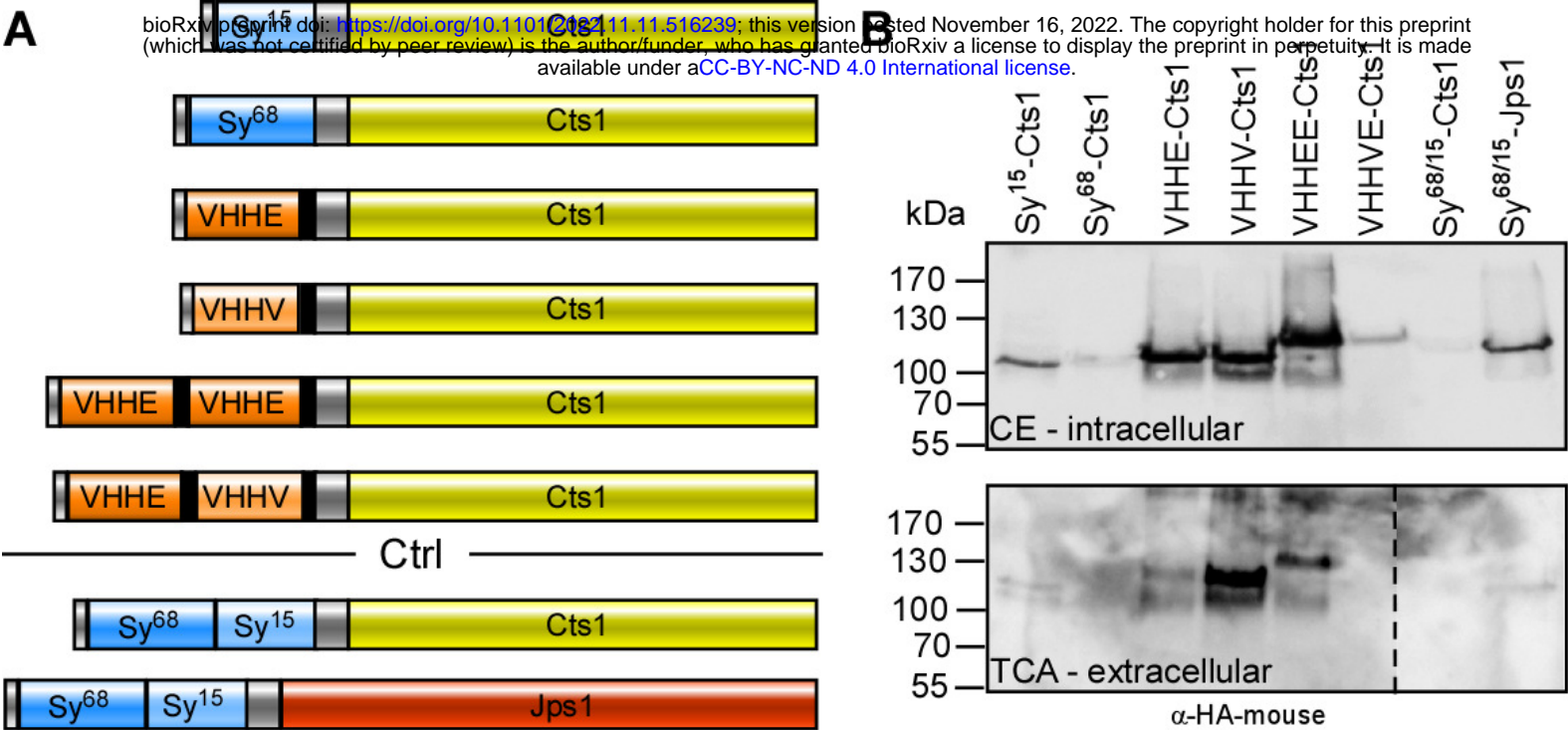752   Epub 2016/09/26 DOI: 10.1007/978-1-4939-3804-9_10

753 **Sun X, Yang S, Al-Dossary AA, Broitman S, Ni Y, Guan M, Yang M, Li J**. (2022). Nanobody-
754   Functionalized Cellulose for Capturing SARS-CoV-2. *Appl Environ Microbiol*. Mar
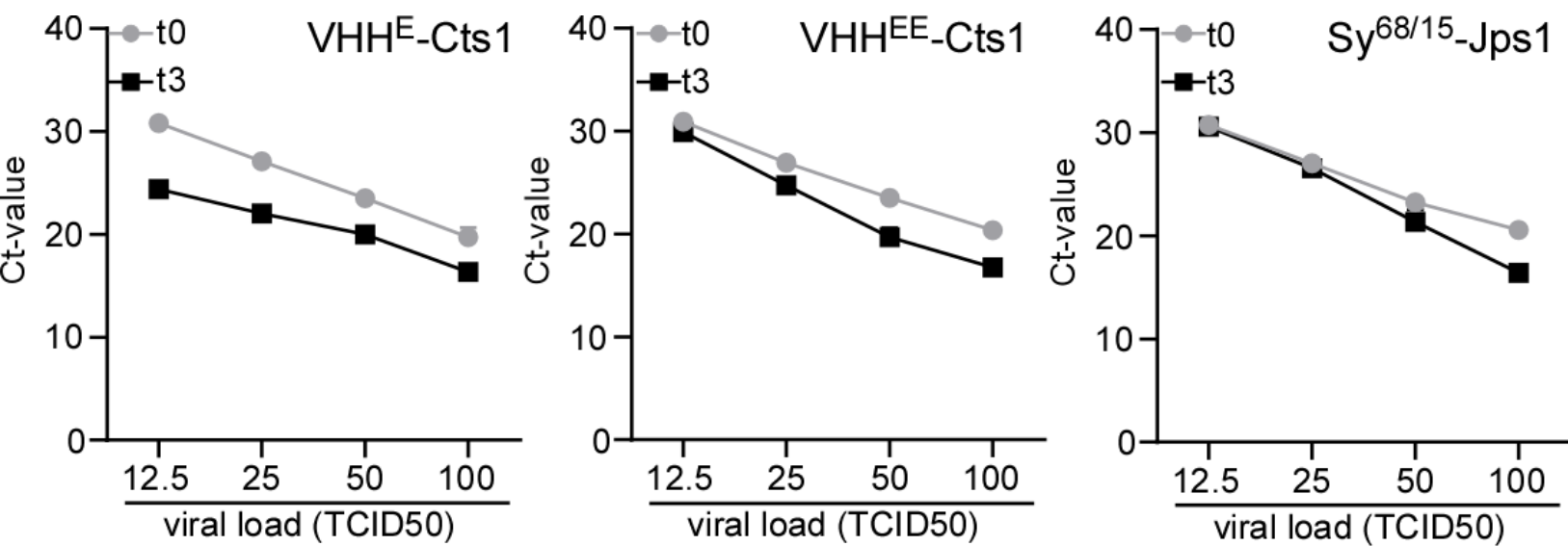755   8;**88**:e0230321. Epub 20220105 DOI: 10.1128/aem.02303-21

756 **Sun Y, Ho M**. (2020). Emerging antibody-based therapeutics against SARS-CoV-2 during the global
757   pandemic. *Antib Ther*. Dec;**3**:246-256. Epub 2021/04/30 DOI: 10.1093/abt/tbaa025

Terfrüchte M, Reindl M, Jankowski S, Sarkari P, Feldbrugge M, Schipper K. (2017). Applying Unconventional Secretion in Ustilago maydis for the Export of Functional Nanobodies. *Int J Mol Sci*. Apr 29;**18**. Epub 2017/05/05 DOI: 10.3390/ijms18050937

Terfrüchte M, Wewetzer S, Sarkari P, Stollewerk D, Franz-Wachtel M, Macek B, Schleputz T, Feldbrugge M, Buchs J, Schipper K. (2018). Tackling destructive proteolysis of unconventionally secreted heterologous proteins in Ustilago maydis. *J Biotechnol*. Oct 20;**284**:37-51. Epub 2018/08/01 DOI: 10.1016/j.jbiotec.2018.07.035

Torjesen I. (2021). Covid-19: Omicron may be more transmissible than other variants and partly resistant to existing vaccines, scientists fear. *BMJ*. Nov 29;**375**:n2943. Epub 20211129 DOI: 10.1136/bmj.n2943

VanBlargan LA, Errico JM, Halfmann PJ, Zost SJ, Crowe JE, Jr., Purcell LA, Kawaoka Y, Corti D, Fremont DH, Diamond MS. (2022). An infectious SARS-CoV-2 B.1.1.529 Omicron virus escapes neutralization by therapeutic monoclonal antibodies. *Nat Med*. Jan 19. Epub 20220119 DOI: 10.1038/s41591-021-01678-y

Walls AC, Park YJ, Tortorici MA, Wall A, McGuire AT, Veesler D. (2020). Structure, Function, and Antigenicity of the SARS-CoV-2 Spike Glycoprotein. *Cell*. Apr 16;**181**:281-292 e286. Epub 20200309 DOI: 10.1016/j.cell.2020.02.058

Walter JD, Hutter CZ, I. Wyss, M.; , Earp J, Egloff P, Sorgenfrei MH, L. M. Gonda, I. , Meier G, Remm ST, S. Plattet, P. , Seeger MA. (2020). Sybodies targeting the SARS-CoV-2 receptor-binding domain. *bioRxiv*. DOI: 10.1101/2020.04.16.045419

Wang Q, Zhang Y, Wu L, Niu S, Song C, Zhang Z, Lu G, Qiao C, Hu Y, Yuen KY, et al. (2020a). Structural and Functional Basis of SARS-CoV-2 Entry by Using Human ACE2. *Cell*. May 14;**181**:894-904 e899. Epub 20200409 DOI: 10.1016/j.cell.2020.03.045

Wang Q, Zhong C, Xiao H. (2020b). Genetic Engineering of Filamentous Fungi for Efficient Protein Expression and Secretion. *Front Bioeng Biotechnol*.**8**:293. Epub 2020/04/24 DOI: 10.3389/fbioe.2020.00293

Weinstein JB, Bates TA, Leier HC, McBride SK, Barklis E, Tafesse FG. (2022). A potent alpaca-derived nanobody that neutralizes SARS-CoV-2 variants. *iScience*. Mar 18;**25**:103960. Epub 20220222 DOI: 10.1016/j.isci.2022.103960

Wrapp D, De Vlieger D, Corbett KS, Torres GM, Wang N, Van Breedam W, Roose K, van Schie L, Team V-CC-R, Hoffmann M, et al. (2020a). Structural Basis for Potent Neutralization of Betacoronaviruses by Single-Domain Camelid Antibodies. *Cell*. May 28;**181**:1004-1015 e1015. Epub 20200505 DOI: 10.1016/j.cell.2020.04.031

Wrapp D, Wang N, Corbett KS, Goldsmith JA, Hsieh CL, Abiona O, Graham BS, McLellan JS. (2020b). Cryo-EM structure of the 2019-nCoV spike in the prefusion conformation. *Science*. Mar 13;**367**:1260-1263. Epub 20200219 DOI: 10.1126/science.abb2507

Xu Y, Xu Y, Bi B, Hou M, Yao L, Du Q, He A, Liu Y, Miao C, Liang X, et al. (2020). A moldable thermosensitive hydroxypropyl chitin hydrogel for 3D cartilage regeneration in vitro and in vivo. *Acta Biomater*. May;**108**:87-96. Epub 20200405 DOI: 10.1016/j.actbio.2020.03.039

Zhong Y, Liu X, Xiao P, Wei S, Wang T. (2011). Expression and secretion of the human erythropoietin using an optimized cbh1 promoter and the native CBH I signal sequence in the industrial fungus Trichoderma reesei. *Appl Biochem Biotechnol*. Nov;**165**:1169-1177. Epub 20110816 DOI: 10.1007/s12010-011-9334-8

801   **Zhuang J, Yin J, Lv S, Wang B, Mu Y**. (2020). Advanced "lab-on-a-chip" to detect viruses - Current
802   challenges and future perspectives. *Biosens Bioelectron*. Sep 1;**163**:112291. Epub 20200512
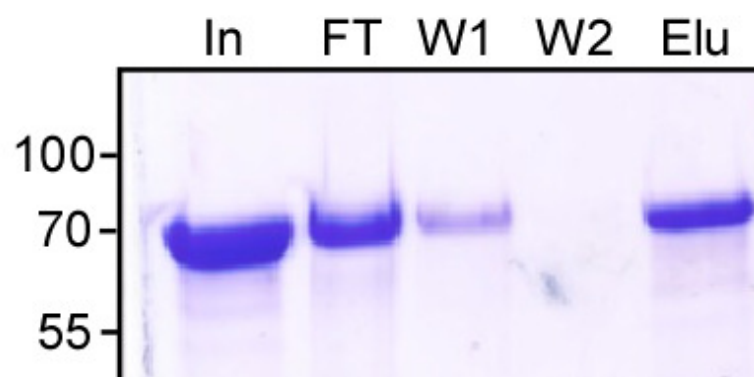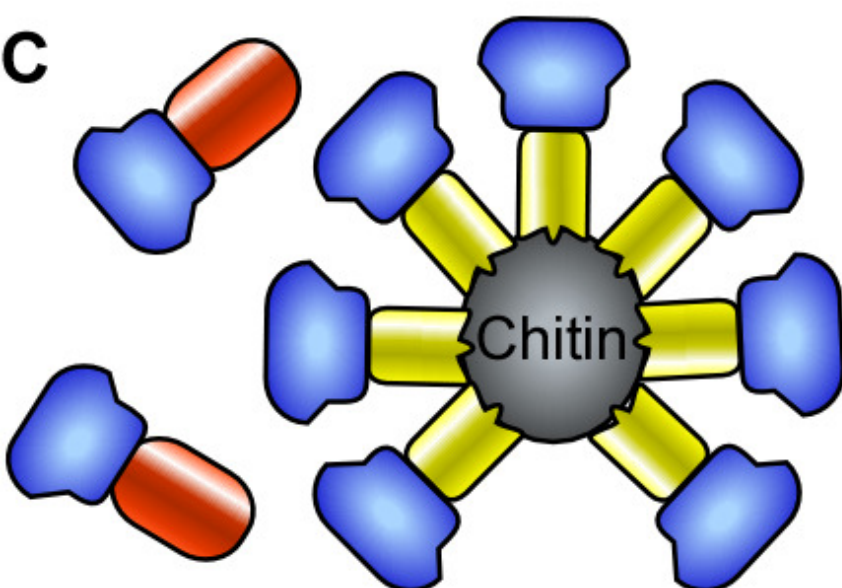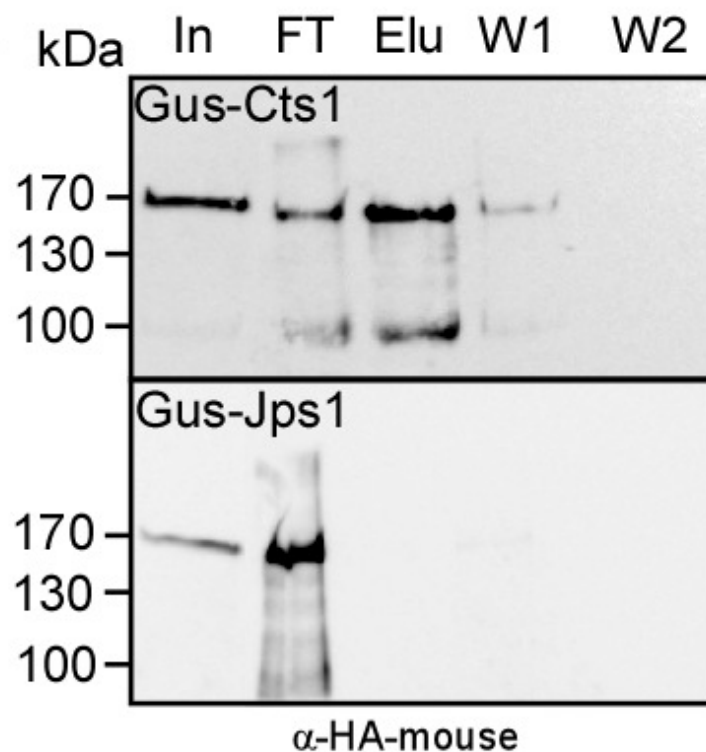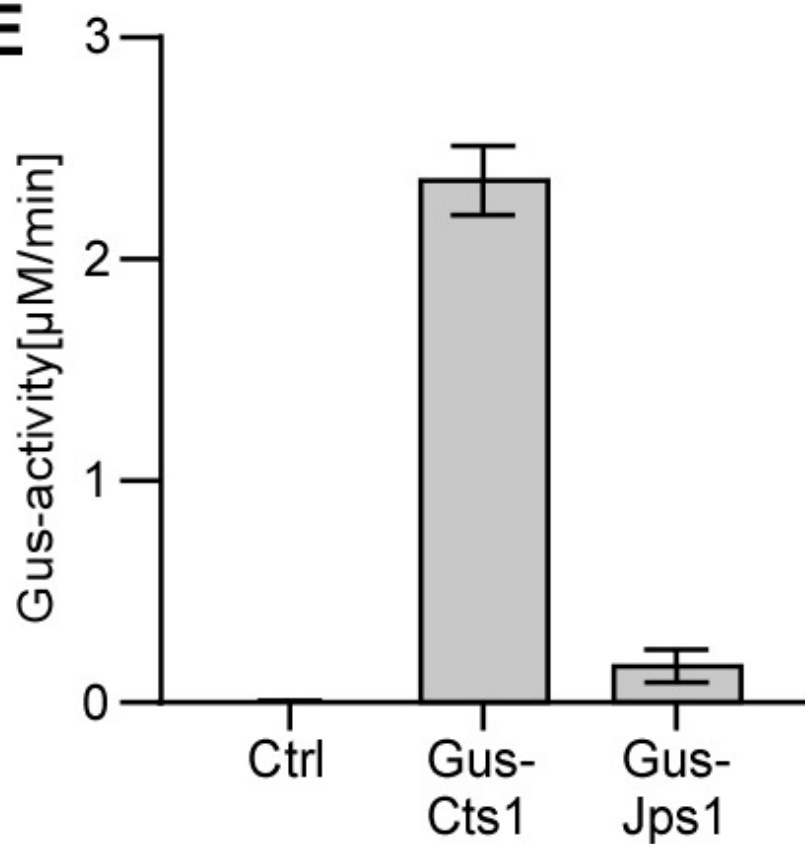803   DOI: 10.1016/j.bios.2020.112291

804

A

B

C

D

α-HA-mouse

E